Experimental Investigation on Convective Heat Transfer of Shear-thinning Fluids by Elastic Turbulence in a Serpentine Channel

Haie Yang[1], Guice Yao[2], Dongsheng Wen[1, 2] *

1 Department of Man-machine Environment Engineering, School of Aeronautic Science and Engineering, Beihang University, Beijing, 100191, China

2 School of Chemical and Process Engineering, University of Leeds, Leeds LS2 9JT, UK

Abstract

Elastic turbulence has shown great potential to enhance heat transfer performance at the microscale. Most of the studies, however, have only considered global convective heat transfer performance along curvilinear channels, despite that the intensity of the chaotic flow varies along the streamline, leading to different local heat transfer characteristics. This work systematically investigated the local convective heat transfer performance by elastic turbulence of a shear-thinning fluid in a serpentine channel. The flow visualization along the serpentine channel was obtained and analyzed to show the existence of elastic instability and elastic turbulence. Significant enhancement of mixing was observed with the increase of polymer concentration and bulk flowrate, suggesting the occurrence of elastic instability and elastic turbulence. The variations of pressure drop, heat transfer coefficients and Nusselt numbers along the serpentine channel were analyzed to reveal local characteristics of elastic turbulence. A three-stage pressure drop profile was identified due to the variations of viscosity and elastic turbulence intensity at different flowrates and Reynolds numbers. A non-linear heat transfer performance, which increased with the increase of polymer concentrations, was observed. These are mainly attributed to the increasing intensity of elastic instability, resulting from the balance between normal stresses and streamline curvatures. A large increase of Nusselt number versus Weissenberg number was also revealed due to the coupling of shear-thinning behavior and elastic instability effects.

Keywords: Elastic turbulence; Shear-thinning fluid; Convective heat transfer; Serpentine channel; Viscoelastic fluids; Flow visualization

List of symbols

a	mm	The width and height of the serpentine channel
A_c	mm^2	Cross-sectional area
A_h	mm^2	Wetting area
A_{heated}	mm^2	The area of the heated surface
b		Fitting index in the C-Y model
c	ppm	Polyacrylamide concentration within working fluids
c_0	ppm	Concentration of the fluorescent FWT red tracer dye

c_p	J/(kg · K)	Specific heat
D_h	mm	Hydraulic diameter of the channel
f		Darcy friction factor
Gz		Graetz number
G'	Pa	Storage modulus
G''	Pa	Loss modulus
h	J/(m^2·s· K)	Local heat transfer coefficient
k	W/(m· K)	The thermal conductivity of the fluids
L	M	The equivalent length of the serpentine channel
M_w	Da	Molecular weight
n		Fitting index in the C-Y model
N		Number of curves in the serpentine channel
Nu		Nusselt number
$P_{1,2,3,4}$	kPa	Position 1, 2, 3, 4 of the test section
P_{in}	kPa	Pressure of the inlet reservoir
P_{out}	kPa	Pressure of the outlet reservoir
Pr		Prandtl number
q	J/(m^2·s)	Heat flux
Q_a	J	The absorbed heat by the fluids
R_c	mm	Center radius of the curves in the serpentine channel
R_{in}	mm	The inner radius of the serpentine channel
R_{out}	mm	The outer radius of the serpentine channel
Re		Reynolds number
S_c	mm	Cross-sectional perimeter
S_h	mm	Wetting perimeter
T_{in}	K	Inlet mean temperature
T_{out}	K	Outlet mean temperature
T_w	K	Wall temperature
T_f	K	Fluid temperature
T_1	K	Temperature of the 1st test point
T_2	K	Temperature of the 2nd test point
T_3	K	Temperature of the 3rd test point
T_4	K	Temperature of the 4th test point
V_V	μl/min	Volumetric / Bulk flowrate
Wi		Weissenberg number
Wi_c		Critical Weissenberg number
x	mm	Distance from inlet of test section to tested point
x_{in}	mm	The inlet length of the serpentine channel

X/a		Dimensionless axial distance
α	m^2/s	Fluid thermal diffusivity
$\dot{\gamma}$	s^{-1}	Shear rate
$\dot{\gamma}_{CY}$	s^{-1}	Shear rate used int the C-Y model
η_0	Pa · s	Viscosity at the zero shear rate
η_{CY}	Pa · s	Viscosity estimated by the C-Y model
η_∞	Pa · s	Viscosity of the infinite shear rate
λ_0	s	The longest relaxation time
ν	m^2/s	Fluid kinematic viscosity
ρ	kg/m^3	Density
Φ	J	The total heat flux
ΔP	kPa	Pressure drop between the inlet and outlet

1 Introduction

Micro/nanoscale flow is a typical phenomenon in many fields including process intensification, micro-reactors, compact heat exchangers, MEMS (micro-electro-mechanical systems), enhanced oil recovery, and drug delivery[1–3]. For micro-flow systems such as MEMS, their increased specific surface area due to the size reduction has brought many advantages in promoting mixing and enhancing mass transport and reaction rate. However for the same reason, the small flow geometry leads to a small Reynolds number ($Re = \rho V D_h/\eta$), which limits the flow pattern to the laminar flow regime for Newtonian fluids, resulting in limited heat transfer performance. Inefficient heat supply or heat dissipation could seriously deteriorate the performance of these devices[4,5]. Increasing Reynolds number by increasing flow velocity, in most of systems, is however not feasible due to the extra pumping power or large pressure drops associated. How to increase the heat transfer performance in laminar flow regime still presents as a big challenge.

A few concepts have been proposed to induce turbulent-like flow in laminar flow regime including mechanical and structural methods[5–9], which have limited success. Viscoelastic fluids, especially shear-thinning fluids and Boger fluids, have been recently found to be able to induce turbulence at the microscale due to the coiling and stretching of polymers inside, which is called elastic turbulence[10]. Elastic turbulence is a turbulence-like phenomenon in extremely low Reynolds number and high Weissenberg number, $Wi = \lambda\dot{\gamma}$, in the flow of viscoelastic fluids, including shear-thinning fluids and Boger fluids as firstly reported by Groisman and Steinberg in 2000[10]. Three main features, all of which are analogous to hydrodynamic turbulence, were found for this turbulent-like flow: pronounced growth of flow resistance, algebraic decay of angular velocity spectra over a wide range of time scales, and orders of magnitude higher mixing performance compared with Newtonian solvent solely. Following this pioneering work, it was found that elastic turbulence could exist in many different geometries, such as the Karman swirling flow[10–13], Taylor-Couette flow[14], flow in serpentine channels[14–20] and flow in a straight channel with an array of pin-protrusions[21,22]. The mechanism of elastic turbulence was also investigated by experimental[23–25] and theoretical[26,27] studies and the intensification of flow was ascribed to the coiling and stretching of polymers in the fluids.

A majority work of elastic turbulence has been focused on the enhanced mass transfer and mixing effects[11,15,17,18,28–31]. For example, Victor Steinberg et al.[11,15,18,28] firstly proposed the potential of effective mixing by elastic turbulence, and Casanell et al.[32] showed that shear-thinning characteristics could lead to enhancement of elastic turbulence intensity. Poole et al. [33] illustrated that the elastic turbulence can be used to create emulsions and enhance mass transfer from immiscible viscous liquids in a simple shear mixing device.

The investigations into convective heat transfer by elastic turbulence is a recent development, including the convective heat transfer in serpentine channels and between two parallel disks, i.e., the Von Karman flow. Heat transfer by elastic turbulence within the flow between two parallel disks was firstly experimentally investigated by Traore et al.[34] using viscoelastic fluids (i.e., a 100 ppm anionic polyacrylamide (PAAm) solution with the molecular weight $M_w = 22\times10^6$ Da in 65%wt aqueous sugar solution) in low Reynolds number flow with negligible inertial instability. A four-time enhancement of heat transfer performance by the viscoelastic fluids compared to that of the Newtonian fluids (i.e., 65%wt aqueous sugar solution) was observed. Such enhancement is comparable to the efficiency increase observed in the case of inertial turbulence at $Re = 1600$. Besides the Von Karman flow, convective flow and heat transfer in serpentine channels has been recently investigated. Li et al.[35–37] investigated the heat transfer performance inside a square cross-section (200 μm×200 μm) micro serpentine channel using the shear-thinning fluids, which were prepared by dissolving a small amount (200, 300 and 400 mg/L concentration all by weight) of nonionic polyacrylamide (NPAM) with the molecular weight of $M_w = 18\times10^6$ Da into deionized water. In their studies, the heat transfer performance was compared with that of the aqueous sucrose solution with 50 % mass concentration over a range of Weissenberg number from 0.1 to 12 due to the similar viscosity. A critical Weissenberg number, $Wi_c = 2.1$, was observed, above which the global Nusselt numbers increased sharply with Wi. Furthermore, the Nusselt number reached to two orders of magnitude for viscoelastic fluids at $Wi > Wi_c$, showing the potential of heat transfer enhancement by elastic turbulence. Abed et al.[19,20] also conducted a set of experiments to study the convective heat transfer in a square cross-section (1 mm×1 mm) serpentine channel using two groups of viscoelastic fluids, i.e., shear-thinning solutions (50 ppm, 100 ppm and 200 ppm PAAm solutions in the mixture of 10% distilled water and 90% glycerin), and approximately constant-viscosity elastic solutions, usually called Boger fluids made of 80 ppm, 120 ppm and 500 ppm PAAm in aqueous solution of 65% sucrose and 1% sodium chloride (NaCl). The results showed that compared to the equivalent Newtonian fluid flow, the convective heat transfer of polymer solutions could be enhanced by 2 - 4 times at low Graetz number Gz (up to 14.6) over a range of Weissenberg number (from 4 to 211). These prior studies have shown that elastic turbulence can enhance mass transfer and the mixing effect, as well as the overall heat transfer performance. It has been found that [19,20,35–37] in elastic turbulence, three main issues, i.e., induction effects, solute effects and solvent effects, could affect the heat transfer performance greatly. As the evolution of elastic turbulence in curved channels is highly dependent on the variation of curvatures, the heat transfer performance along the channel should be different. However, only a global Nusselt number or a self-defined heat intensity was used to characterize the heat transfer effect in either serpentine channels or swirling flow configurations. The local heat transfer discrepancy due to the evolution of the elastic turbulence has not been revealed. In addition, a constant wall temperature boundary condition was mainly adopted previously, while in many applications constant heat flux is

applied.

Addressing these limitations, this work aims to conduct a fundamental study to reveal local heat transfer characteristics of elastic turbulence utilizing shear-thinning fluids along serpentine channels under a constant heat flux q condition. The wall temperature along a serpentine channel and temperature of the inlet and outlet were measured experimentally, and the pressures of the inlet and outlet were recorded synchronously. Different concentrations of aqueous solutions of anionic polyacrylamide (PAAM, 200 ppm, 500 ppm and 800 ppm) were used as working fluids. The dependence of pressure drops on flowrate and the relation of heat transfer performance to Reynolds number (i.e., from 0.1 to 2.6) and Weissenberg number (i.e., from 0.8 to 148.3) were obtained to illustrate the local mechanism of heat transfer performance in elastic turbulence.

2 Experimental measurement

2.1 Experimental system

The experimental system is shown schematically in Fig. 1, which contains a flow unit, a heating unit and a measurement unit. The flow unit includes a syringe pump, a test section and a collection tank. A syringe pump (KD Scientific, U.S.A) was used to control the bulk flow rates. The test section was a copper serpentine channel mounted on an ABS (Acrylonitrile Butadiene Styrene plastic) plastic frame. As shown in Fig. 2, the channel had a length of 77 mm and inner and outer radius of 1 mm and 2 mm, respectively. The path length of the serpentine channel is 94.2 mm in the test section. The heating unit has a DC power supply, a heating surface and an insulating cover. A DC Power supply (National Instrument RMX-4126, U.S.A) can provide a variable heat input and a constant power of 6.28 W is applied in the experiments. A flexible heating tape was placed on the sub surface of the copper channel with the same width and height of the channel. in order to do the best to ensure that the right and left surface are heated uniformly, some slim micro channels are carved at the bottom of the copper test section and paralleled with the streamlines of the serpentine channel to insure that most of the thermal energy spread vertically and to avoid horizontal heat loss. The insulating materials (Armaflex, Germany) with a 10 mm thickness were used to surround the copper channel to prevent heat dissipation (as showed in Fig. 2). The detailed illustration of the serpentine channel is shown in Fig. 2. The right, left and bottom surfaces were heated while the up surface was insulated. The measurement unit contains a data acquisition system, thermocouples, pressure sensors and a computer. Four T-type thermocouples (Omega TT-T-36-SLLE, U.S.A) were located at the distance of 14.13 mm(T_1), 37.68 mm(T_2), 61.23 mm(T_3), and 84.78 mm(T_4), respectively, from the inlet of the test section (as shown in Fig. 2). They were inserted into the small hole of 0.5 mm radius in the both sides of the copper channel to measure the wall temperatures along the channel. Two other thermocouples were mounted into the inlet and outlet of the reservoirs separately to measure the bulk temperature of working fluids. The thermocouples with accuracy of 0.1 K were calibrated before the experiments. Two pressure sensors (Xin Hai Zhong Feng, 0-10 kPa, C.N.) were installed on the both sides of the plastic frame (as shown in Fig. 2) to measure the pressure drop along the channel. A data acquisition system (Agilent 39470A, U.S.A), which was connected to a computer, was used to collect and store data.

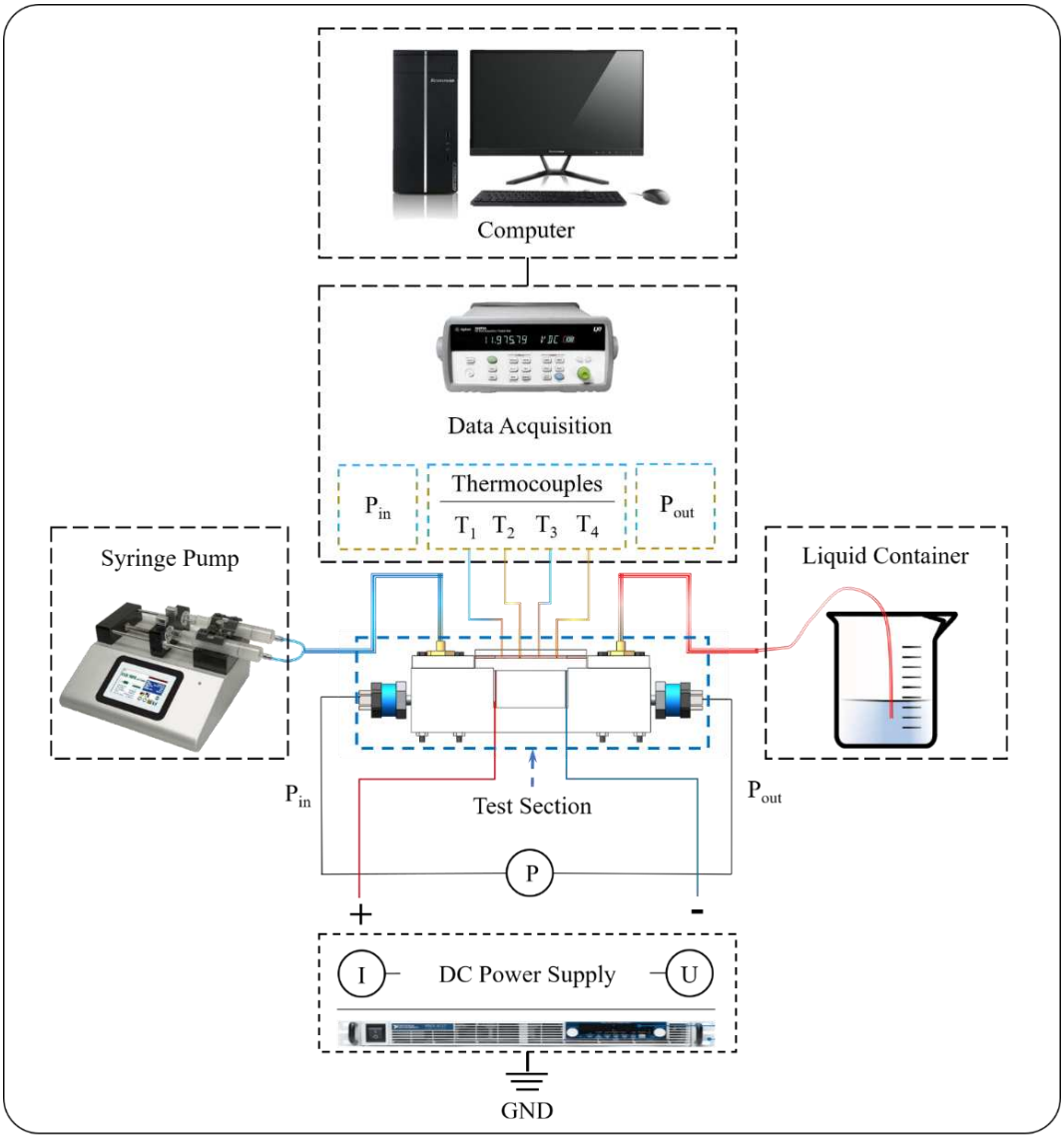

Fig. 1 Experimental system

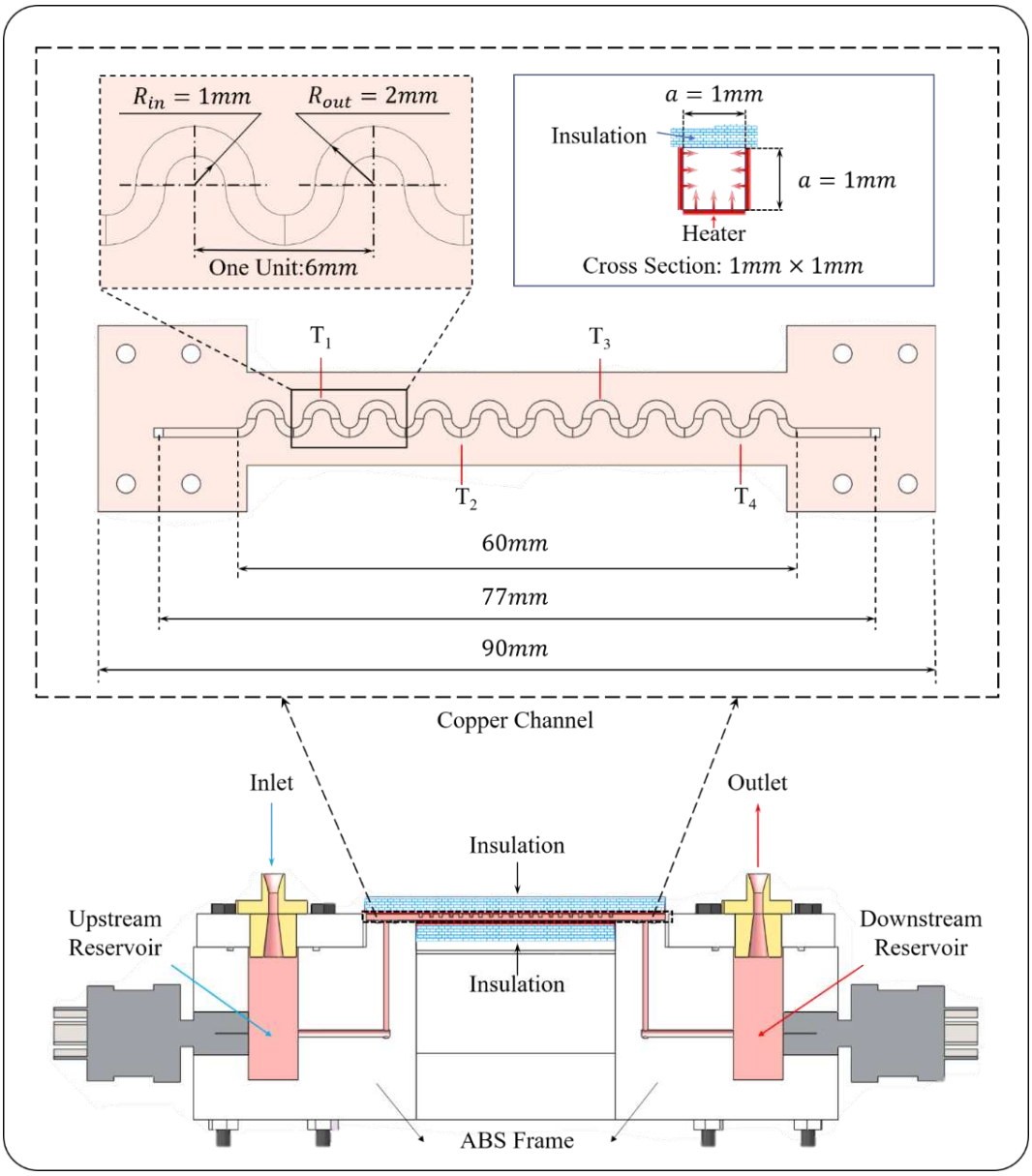

Fig. 2 The dimension and boundary condition of the serpentine channel

2.2 *Flow visualization apparatus and procedures*

The apparatus employed for flow visualizations is shown in Fig. 3. The associated test serpentine channel is made by the combination of optically clear acrylic glass (PMMA) and cooper. The flow unit includes two syringe pumps, a test section and a collection tank. Two syringe pumps (KD Scientific, U.S.A) was used to control the bulk flow rates of the working fluids and the staining fluids, respectively. The working fluids here are the deionized water and PAAM (polyacrylamide, M_w = 18,000,000 Da, Xi Long Chemistry Inc, China) aqueous solutions with the concentration of 200 ppm, 500 ppm, 800 ppm, respectively. To provide constant in the channel, the staining fluids are prepared by dissolving Kingscote fluorescent FWT red tracer dye[38] into the working fluids with a concentration of c_0 = 5 ppm and injected into the test section by the syringe pump at rates from 8.3 to 145.7 μl per minute. The syringe is connected through tubing to a needle positioned in the point of the serpentine channel which is the top peak point of the first semi-loop in the serpentine channel (as shown in Fig.

3). The test section has the same scale in comparison with the device utilized for the experiments of heat transfer (as shown in Fig. 2). The device is kept constant level throughout testing to minimize variations due to hydrostatic pressure and gravity. A high speed camera (I-SPEED 720, U.K.) is used to record images of the channel at a rate of 30 frames per second. The spatial resolution of test window used here in the images is 640 × 480 pixel.

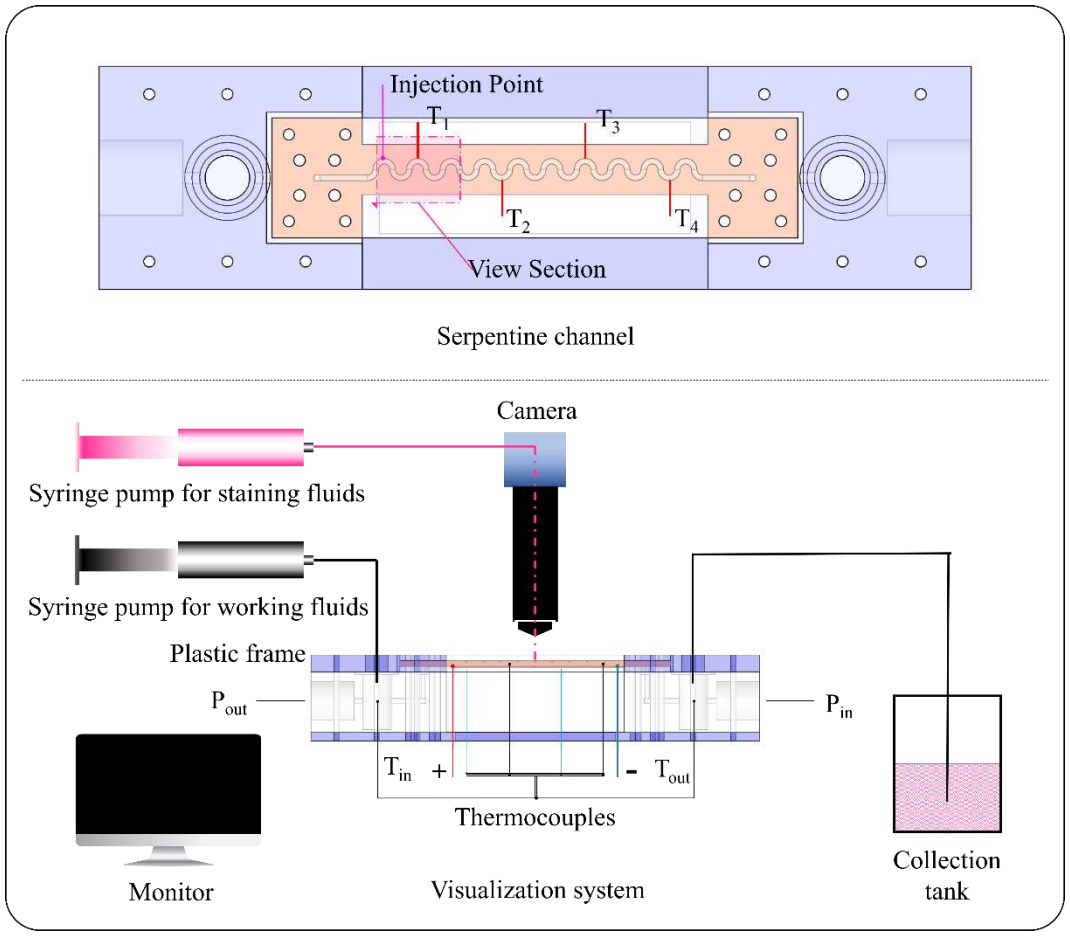

Fig. 3 The flow visualization device with dye injection

2.3 Data processing

The heat transfer performance by elastic turbulence using shear-thinning fluids is quantified by the local convective heat transfer coefficient h (Eq.(1)) and Nusselt number Nu (Eq.(2)), as defined:

$$h(x) = \frac{q}{T_w(x)-T_f(x)} \quad (1)$$

$$Nu(x) = \frac{h(x)D_h}{\lambda} \quad (2)$$

where q is the heat flux, $T_w(x)$ and $T_f(x)$ are the local wall temperature and fluid temperature, respectively. x is the distance from the inlet of the test section (as shown in Fig. 2) to the tested point

which is calculated by Eq.(3):

$$x = 2\pi NR_c + x_{in} \quad (3)$$

where N is the number of curves in the serpentine channel from the beginning point of the curves to the test point of the thermocouple, R_c is the center radius of the curves in the serpentine channel. x_{in} is the inlet length of the serpentine channel which is from the center point of the inlet to the beginning point of curves. D_h is the hydraulic diameter of the channel, and k is the thermal conductivity of the fluids. The hydraulic diameter of the channel D_h is defined as Eq.(4):

$$D_h = \frac{4A_h}{S_h} \quad (4)$$

where A_h is the wetting area and S_h is the wetting perimeter. The heat flux q is calculated by Eq.(5):

$$q = \frac{\Phi}{A_{heated}} \quad (5)$$

where Φ is the total heat flux which is defined by the energy conservation $\Phi = Q_a$, and A_{heated} is the area of the heated surface. Q_a is the absorbed heat by the fluids which can be estimated utilizing Eq.(6):

$$Q_a = c_p \rho V_V (T_{out} - T_{in}) \quad (6)$$

where c_p is the specific heat, ρ is the density of working fluids, V_V is the volumetric flowrate, and T_{out} and T_{in} are the inlet and outlet temperature, respectively. The local fluid temperature is estimated using energy balance Eq.(7):

$$T_f(x) = T_{in} + \frac{qS_c}{\rho c_p V A_c} x \quad (7)$$

where A_c and S_c are the cross-sectional area and perimeter of the heated length of the channel respectively, and V is the mean fluid velocity of the fluids. The assumption of no heat loss in the insulation layer is utilized as the basis of Eq.(7). The error of this assumption is estimated by comparing the measured inlet and outlet temperature differences with theoretical values calculated by Eq.(7). In this work, the deviation was found to be less than 0.02%.

In this study, the parameters measured directly contains the inlet temperature T_{in} and the outlet temperature T_{out} of working fluids, wall temperatures T_w along the serpentine channel, the inlet pressure P_{in} an outlet pressure P_{out}, and flowrate V lists the maximum errors of these parameters, which combine system errors and random errors by using root-sum-square (RSS) approach[35] (See details in Table 1).

Table 1 Ranges and maximum errors of experimental parameters in experimental conditions

Parameter	Maximum Error	Ranges of Parameters

Temperatures	T_{in}	K	0.1K	299.2- 200.6K
	T_{out}			205.2 - 314.4K
	T_w			For water: 331.7 – 352.5K For polymer solutions: 303.4 - 319.7K
Pressures	P_{in}, P_{out}	Pa	0.1 kPa	Range of pressure drop: 0.1 - 8.6 kPa
Flowrate	V	μl/min	0.01 μl/min	200 - 3500 μl

To evaluate the flow performance, the friction factor f of the flow of shear-thinning fluids within the serpentine micro-channel is defined as:

$$f = \frac{\Delta P}{\frac{1}{2}\rho V^2} \cdot \frac{D_h}{L} \quad (8)$$

where L is the equivalent length of the serpentine channel, ΔP is the pressure drop between the inlet and outlet of the serpentine channel.

For shear-thinning fluids, the Nusselt number is related to the Reynolds number Re, the Prandtl number Pr, the Weissenberg number Wi and the Graetz number Gz which are defined as Eq.(9) (10)(11) and Eq.(12), respectively.

$$Re = \frac{\rho V D_h}{\eta} \quad (9)$$

$$Pr = \frac{v}{\alpha} \quad (10)$$

$$Wi = \lambda \dot{\gamma} \quad (11)$$

$$Gz = \frac{Re\, Pr\, D_h}{L} \quad (12)$$

where η is the fluid dynamic viscosity which is the viscosity of the shear-thinning fluids in the specific bulk flowrate at the averaged inlet and outlet temperatures along the serpentine channel in this study, v is the fluid kinematic viscosity, α is the fluid thermal diffusivity which is defined as $\alpha = k / (\rho c_p)$, λ is the longest relaxation time of the working fluids which is the longest relaxation time of the average temperature of all the tested temperatures in this study since that the relaxation time is negligibly influenced by temperature variations within the range of covered temperatures according to the curves of the relaxation time against the angular frequency which are illustrated in the next section *2.4 Polyacrylamide polymer solutions*, and $\dot{\gamma}$ is the shear rate which is calculated by $\dot{\gamma} = V/D_h$, where D_h is the hydraulic diameter of the channel.

2.4 Polyacrylamide polymer solutions

Aqueous solutions of PAAM (Anionic Polyacrylamide, M_w = 18,000,000 Da, Xi Long Chemistry Inc, China) are utilized with for different polymer concentrations: 0 ppm, 200 ppm, 500 ppm, 800 ppm,

where ppm refers to parts per million. As such, the 0 ppm arrangement is utilized with a aqueous solution (without added polymers) to create a Newtonian solution with an approximately constant viscosity that is independent of shear rate. the shear-thinning solutions are then prepare by adding polymer powder into the deionized water. When each solution is prepared, the appropriate polymer concentration (as qualified using PAAM) is employed. The procedure for mixing the stock solution is adopted from Groisman et al.[14] and Abed et al.[20] . A stock solution of PAAM was prepared and used for the entire experiments. First we dissolved 1.5 g of PAAM powder in 300 ml of deionized water by gentle shaking for 3 h. Next deionized water was added up to prepare 500 g stock polymer solution. The polymer solution is gently mixed for another 3h in a commercial mixer propeller at moderate speed. After the preparation of a stock solution, for example, to mix a 200 ppm solution, 33.33 g of the stock solution was dissolved in 300 ml of deionized water and then the deionized water is added up to prepare 500 g polymer solution with the concentration of 200 ppm, as the solution is gently mixed for 4 h in a commercial mixer with propeller at a moderate speed.

The addition of small amount of PAAM has been found negligible influence on the specific heat c_p and the thermal conductivity k, including 200 ppm / Water, 500ppm / Water and 800 ppm / Water (see data in Table 2), comparing to Newtonian fluids (Deionized water) according to the measurements by Abed et al.[20] and Li et al. [35] while the fluid dynamic viscosity η and the longest relaxation time λ of shear-thinning fluids (200ppm / Water, 500 ppm / Water, and 800 ppm / Water) are quite different from the Newtonian fluid (Deionized water). A range of systematical experiments have been conducted for measuring the viscosity η and longest relaxation time λ of the PAAM aqueous solutions by Abed et al.[20], Li et al.[35,36] and Qin et al.[21]. However, since that the study was conducted using shear-thinning fluids, which are PAAM aqueous solutions with the concentration of 200 ppm, 500 ppm, and 800 ppm, respectively, which are neither the same as working fluids used by Li et al.[35,36] nor Abed et al.[20] , the precise measurements of rheological properties of the working fluids are important in this study.

The rheological properties including the viscosities and the relaxation time of the shear-thinning fluids were measured by a rheometer (TA Instruments AR100 N, U.S.A) controlled stress rheometer with a stainless steel cone-and-plate plate geometry (40 mm diameter, 2° cone angle) with an uncertainty in viscosity of ±2°[39] at the temperatures of 293K, 298K, 303K, 308K, 313K, 318K, respectively. In this study, the shear viscosity, η, for all shear-thinning fluids against shear rate is schematically illustrated in Fig. 4. It is shown that the shear viscosity of shear-thinning fluids have significant shear-thinning behavior. The Carreau-Yasuda model was adopted to fit the experimental viscosity data[20]:

$$\eta_{CY} = \eta_{\infty} + \frac{(\eta_0 - \eta_{\infty})}{[1 + \dot{\gamma}_{CY}{}^{b}]^{n/b}} \qquad (13)$$

where η_{CY} is the viscosity estimated by the C-Y model, η_0 is the viscosity at the zero shear rate and η_{∞} is the viscosity of the infinite shear rate, $\dot{\gamma}_{CY}$ is the shear rate used int the C-Y model, and b, n are a fitting parameter and a fitting index in the C-Y model, respectively.

In order to measure the precise relaxation time, small amplitude oscillatory shear stress (SAOS) tests were conducted by the rheometer for the measurements of the storage modulus, G', which

represents the energy of elastic storage and the state of the structured materials, and the loss modulus, G'', which represents viscous dissipation or loss of energy[20]. Frequency sweeps were conducted within the linear viscoelastic region when the oscillation shear stress is kept constant at a low value which is 0.01 here. Fig. 5 shows the dependence of polymer relaxation time on the angular frequency from the measurements of SAOS for all shear-thinning fluids used in this study which are PAAm aqueous solutions with the concentrations of 200 ppm, 500 ppm, 800 ppm at the temperatures of 293K, 298K, 303K, 308K, 313K, 318K, respectively (as shown in Fig. 5).

From Fig. 5 (a) (b) (c), it is obvious that temperature variations in the range of degrees from 293K to 318K have a slight influence on relaxation time. Therefore, the averaged relaxation time of the working fluid at various temperatures is used to estimate the value of the longest relaxation time, λ_0. The value of the longest relaxation time, λ_0, which are estimated in the limit of the angular velocity approaching to zero are also summarized in Table 2 for all non-Newtonian fluids utilized in the study.

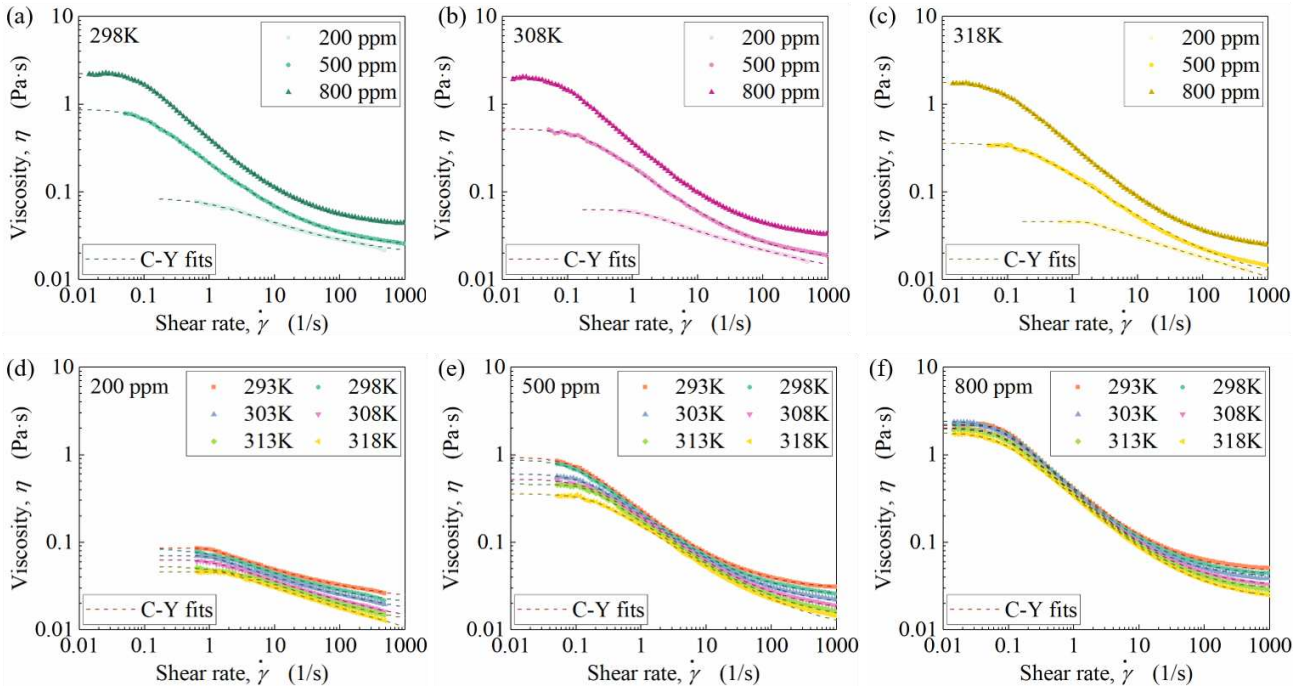

Fig. 4 The viscosity of the shear-thinning fluids versus shear rates, including 200 ppm / Water, 500 ppm / Water, and 800 ppm / Water at the temperature of 293K, 298K, 303K, 308K, 313K, 318K. (a) (b) (c) The dependence of viscosity on the shear rate for different polymer concentrations at the temperatures of 298K, 308K, 318K, respectively. (d) (e) (f) The dependence of viscosity on the shear rate for various temperatures with the concentrations of 200 ppm, 500 ppm, 800 ppm, respectively.

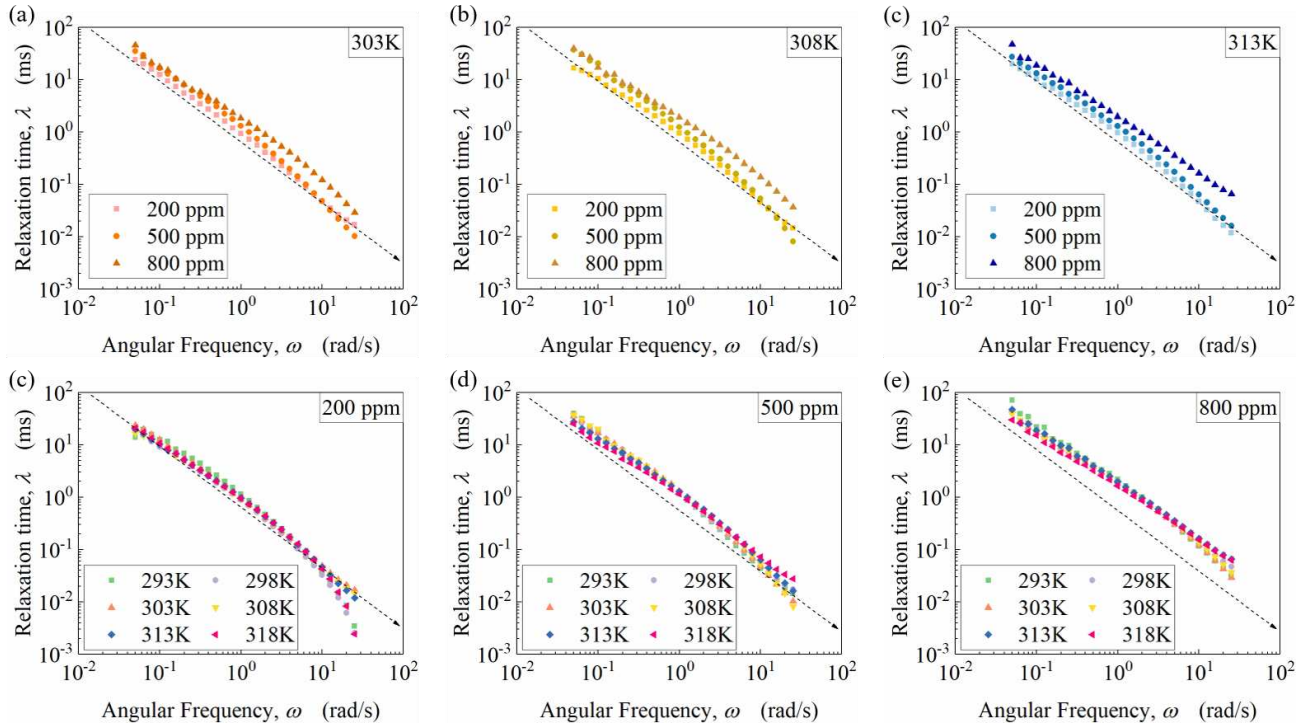

Fig. 5 Relaxation time against the angular frequency obtained from small amplitude oscillatory shear stress measurements for the shear-thinning fluids with the concentrations of 200 ppm, 500 ppm, 800 ppm, respectively, at the temperatures of 293K, 298K, 303K, 308K, 313K, 318K, respectively. (a) (b) (c) The dependence of relaxation time on the angular frequency for different concentrations at the temperatures of 293K, 303K, 313K, respectively. (d) (e) (f) The dependence of relaxation time on the angular frequency for various temperatures with the concentrations of 200 ppm, 500 ppm, 800 ppm, respectively.

Table 2 Thermal properties and zero relaxation time of working fluids

Working fluids	Density	Specific heat	Thermal conductivity	Longest relaxation time
	ρ	c_p	k	λ_0
	kg/m^3	J/(kg·K)	W/(m·K)	s
Deionized water	995	4178	0.615	
200 ppm / Water	996	4178	0.615	0.087
500 ppm / Water	996	4178	0.615	0.101
800 ppm / Water	998	4178	0.615	0.126

2.5 Initial test of the experimental system against water

Before the systematical investigation of heat transfer performance of the shear-thinning fluids, the reliability and accuracy of the experimental system was calibrated utilizing the deionized water as the working fluid. The results were compared with the Shah equation Eq.(12) (as shown in Fig. 6). Reasonably good validation can be seen between the Shah Equation and measured data.

$$Nu = 1.953\,(Re\,Pr\,\frac{D}{x})^{\frac{1}{3}} \qquad (12)$$

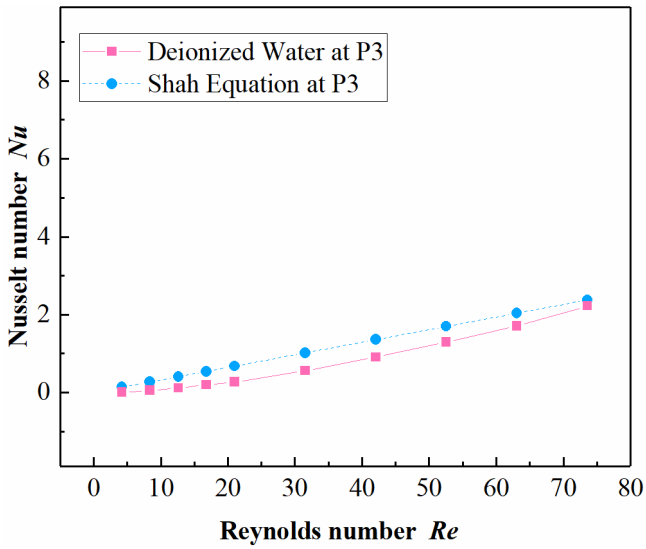

Fig. 6 Comparison with Shah Equation at Position 3 using deionized water

3 Experimental results and discussions

After establishing the confidence of the experimental system, systematical experiments were conducted among the Reynolds number of 0.1 – 2.6 and the Weissenberg number of 0.8 – 148.3 to investigate the flow visualization and heat transfer performance by elastic turbulence in the serpentine channel using three shear-thinning fluids, including 200 ppm / Water, 500 ppm / Water and 800 ppm / Water.

3.1 Flow visualization results

Flow visualization images of the deionized water and for the polymer solutions with the concentrations of 200 ppm and 500 ppm are presented in Fig. 7 in the flow within a serpentine channel. Visualization images of the deionized water in Fig. 7a are given without the addition of polymer powder at the bulk flow rate of 200 μl/min , 1500 μl/min , and 3500 μl/min , respectively. Visualization images of the 200 ppm and 500 ppm polymer solutions in Fig. 7b and Fig. 7c are shown at the same bulk flowrates. These data are obtained using the flow visualization apparatus and procedures which are described above, where dye is injected from the top peak of the first semi-loop in the serpentine channel.

Dye bands of the Newtonian fluid (deionized water) in Fig. 7a are smooth, narrow, and generally well defined with little distortion, as the bulk flow rate changes. Here, dye trajectories follow laminar flow streamlines. As a result, only minimal secondary flows, perturbations and very little augmented mixing exist within the serpentine channel. Some similar experiments had been conducted by Copeland et al.[38] in a one semi-loop channel which is called VDP. However, as schematically illustrated in Fig. 7b and Fig. 7c for the polymer concentration of 200 ppm and 500 ppm, respectively, totally different flow behaviors and flow status do exist. Here, the increased mixing of dye distributions shows mixing and agitation caused by elastic instability and elastic turbulence. The mixing is dramatically enhanced, as evidenced by augmented dye spreading along the serpentine channel. The dye is spread throughout the entire channel, when the bulk flow rate reaches a characteristic magnitude.

Such behavior is associated with enhanced local flow strain, which leads to initial polymer distortion

and agitation, and increased polymer stretching[38] in the direction of the center curvatures of the serpentine channel. Therefore, the resulting increased dye distribution and mixing are related to the transition onset and development of elastic instability and elastic turbulence. In addition, with the increase of polymer concentration, the generation of transition seems to occur at a lower bulk flow rate as showed in Fig. 7b and Fig. 7c, although the natural tendency of increased viscosity for Newtonian fluids is suppression of flow fluctuation as detailed by Copeland et al.[38] . Copeland et al.[38] claimed that the flow variations observed within single semi-section of a serpentine channel (which is VDP in the paper of Copeland et al.[38]) are not due to centrifugal instabilities related to streamline curvature since that in VDP, the related Dean number are not so large to induce centrifugal-instability induced secondary flows. Due to the relatively low Reynolds number and small characteristic scale of the serpentine channel, the Dean number is still not large enough to generate a Dean vortex or induce the centrifugal instability although experiments were conducted within a serpentine channel which had twenty semi-sections as same as a connection of twenty VDP. In addition, the experimental conditions associated with transition also cannot be characterize by one Dean number, and associated Dean number do not vary with polymer concentration. The differences in the flow visualization images between Fig. 7b and Fig. 7c are due to the increased elasticity caused by the enhancement of polymer concentration. Although the enhancement of relaxation time with the increased polymer concentration are moderate, comparing Fig. 7b and Fig. 7c, with the increased polymer concentration, elastic instability is generated in a lower bulk flowrate and the instability of elastic turbulence is reinforced.

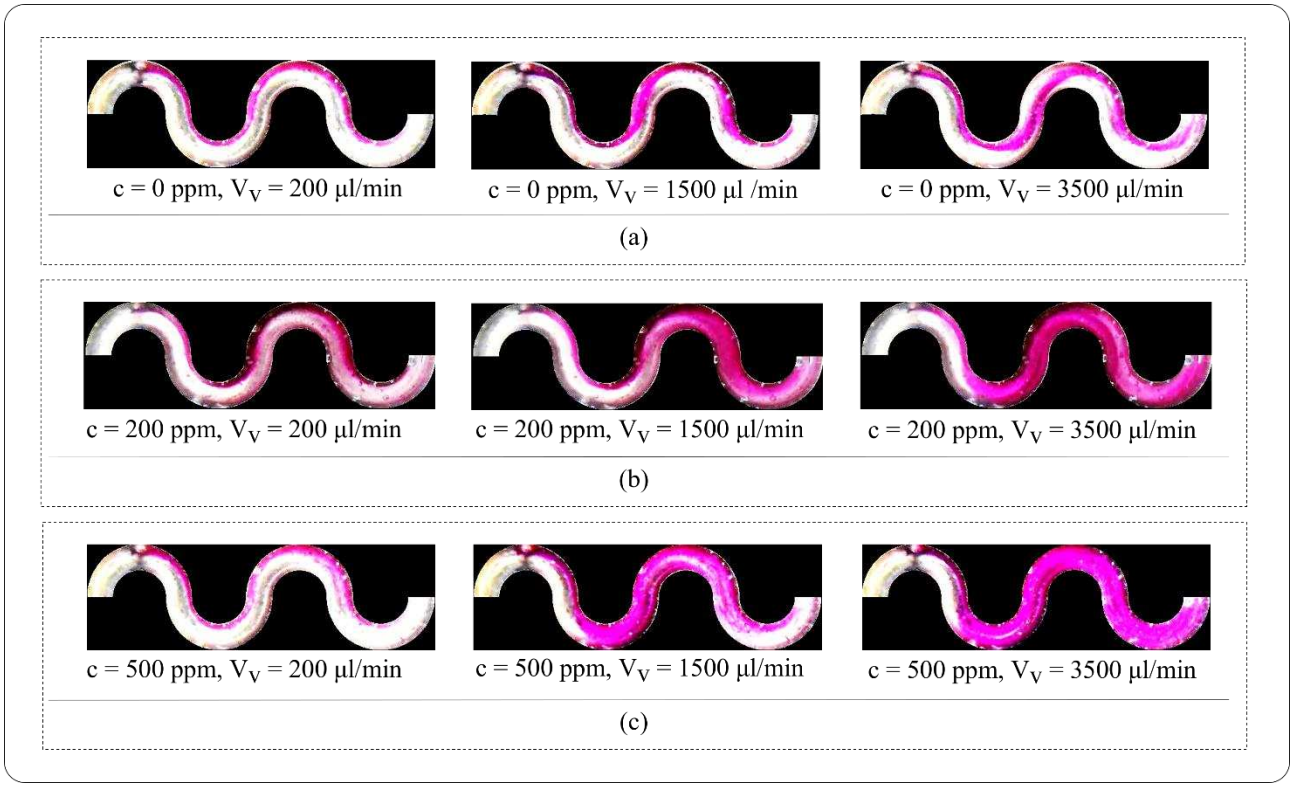

Fig. 7 Flow visualization images. (a) Deionized water only (without the addition of polymer) at the bulk flowrates V_V at 200, 1500, and 3500 µl/min, respectively. (b) 200 ppm PAAm solution at the bulk flowrates V_V at 200, 1500, and 3500 µl/min, respectively. (c) 500 ppm PAAm solution at the bulk flowrates V_V at 200, 1500, and 3500 µl/min, respectively.

3.2 Dependence of the pressure drop on volumetric flowrate and Reynolds number

In analogous with the analysis method by Abed et al.[20], Li et al.[35], and Groisman and Steinberg[14], the dependence of steady-state pressure drop ΔP for shear-thinning fluids and Newtonian fluids on volumetric flowrates V_v between 200 μl/min and 3500 μl/min and relative Reynolds number, respectively, with different polymer concentrations are shown in Fig. 8 (a) , (b) and (c). Here the pressure drop is calculated by the pressure difference between upstream and downstream reservoirs along the serpentine channel for shear-thinning fluids and Newtonian fluids. The results clearly show that the pressure drops of both the Newtonian fluid and shear-thinning fluids increase with flowrates and PAAm concentration. The pressure drop of Newtonian fluids exhibits a linear increase across the whole range of volumetric flow rates because of the laminar flow regime (as shown in Fig. 8(c)), which was also validated by Abed et al.[20], Li et al.[35], and Groisman and Steinberg[14], respectively. However, for viscoelastic fluids, one can see a moderate non-linear growth in low and medium concentration of PAAm (200 ppm / Water, 500 ppm / Water) and a distinct non-linear growth in high concentration of PAAm (800 ppm / Water) of the flow resistance for shear-thinning fluid. The pressure drops indicate a RSR (Rapid-Slow-Rapid) three-stage trend in general for polymer solutions between flowrates 200-3500 μl/min which is associated with Reynolds number in Fig. 8 (b). This non-linear increase for viscoelastic fluids, especially for Boger fluids, was initially proposed by Groisman and Steinberg[14], and was developed in shear-thinning fluids by Abed et al.[20] with the presence of extremely irregular linear trend due to the too wide range of volumetric flowrates. The increase is rapid firstly for the flowrates between 200-1000 μl/min which are associated with relatively low Reynolds number in Fig. 8 (b), then appears slower when the flowrate is between 1000-2000 μl/min referring to the moderate Reynolds number and finally becomes rapid again when flowrates reach 2000-3500 μl/min at high Weissenberg number. Here, since that the range of Reynolds number is from approximately 0.2 to 2.3 for shear-thinning fluids, which means that the influence of inertial effect can be neglected in this investigation. Therefore, for the existing RSR phenomenon, in the range of low flow rate, the rapid enhancement is because that the viscous force is the dominating effect. Since that the viscosity of shear-thinning fluids is much higher than that of Newtonian fluids, a significant trend of increase is observed in the variations of pressure drop of shear-thinning fluids. The fast increase of pressure drops are induced by the higher viscosity of the shear-thinning fluids, which results in a larger friction factor directly attributed to a higher friction resistance since that it is a not negligible term of the pressure drop in a flow along a serpentine channel[35]. When flow rates increase, the ratio of the viscosity of the viscoelastic fluids to that of Newtonian fluids becomes lower due to the shear-thinning phenomenon, which, as a result, leads to a gentle increase comparatively. In the region of high flow rate, a secondary flow accompanied with a coil-stretch transition[13] of long-chain polymers was induced by the interaction of a first normal-stress difference[20] and streamline curvature in the serpentine channel, where the corresponding Reynolds number is still low and the Weissenberg number is high enough.

Since that the Reynolds number here are still lower than 2.7 which is a characteristic Reynolds number of the generation of Dean vortex according to Ligrani et al. [40], the dramatic increase of pressure drop in the rapid third stage are not caused by the Dean effects. In addition, as illustrated in the flow images in the previous section 3.1, one can see that the centrifugal effects have limited influence on the flow status which means that the flow of Newtonian fluids within a serpentine channel

keeps steady and laminar even in a high flowrate (here, V_v = 3500 μl/min). Therefore, it is reasonable that such flow instability is solely driven by elasticity and could induce elastic turbulence over a critical flowrate along the serpentine channel, which results in an increase of flow resistance[14]. Therefore, a RSR (Rapid- Slow- Rapid) three-stage pressure drop do exist in the shear-thinning fluid flow and can be attributed to the high viscosity at low flowrates, shear-thinning properties at medium flowrates and elastic turbulence at high flowrates.

Fig. 8(d) shows the experimental results of Darcy friction factor *f* versus *Re* indicating that the values of friction factor of the Newtonian fluid (deionized water) collapse with the theoretical (Darcy) equation ($f = 57/Re$, for a straight micro channel with a square cross section[41]) for fully-developed isothermal laminar flow (Re = 0.2-6.0). For the Newtonian fluids, the friction factor declines linearly with the enhancement of Reynolds number on a log to log illustration. In Fig. 8 (d) and also the flow visualization images presented in section 3.1, it is obvious that, in this study, the flow of a Newtonian fluid (deionized water) within a serpentine channel behaves like flow in a straight channel since that the viscous forces dominate the flow suppressing the formation of secondary flow[42] which is probably induced by the interaction of large normal stresses with streamline curvature caused by the Dean vortex[40]. Investigations using the Newtonian fluid (deionized water) is a validation of the measurements. Otherwise, the friction factors of the shear-thinning fluids are also illustrated in Fig. 8(d) for the comprehension of elastic turbulence effects. A strongly enhancement of the friction factor of shear-thinning fluids is observed compared with the Newtonian fluids. A secondary flow is seem to develop in the shear-thinning flow owing to the interaction of a first normal stress difference and streamline curvature[20]. However, the large increases in the pressure drop for the shear-thinning fluids are potentially caused by elastic instability and elastic turbulence within the serpentine channel.

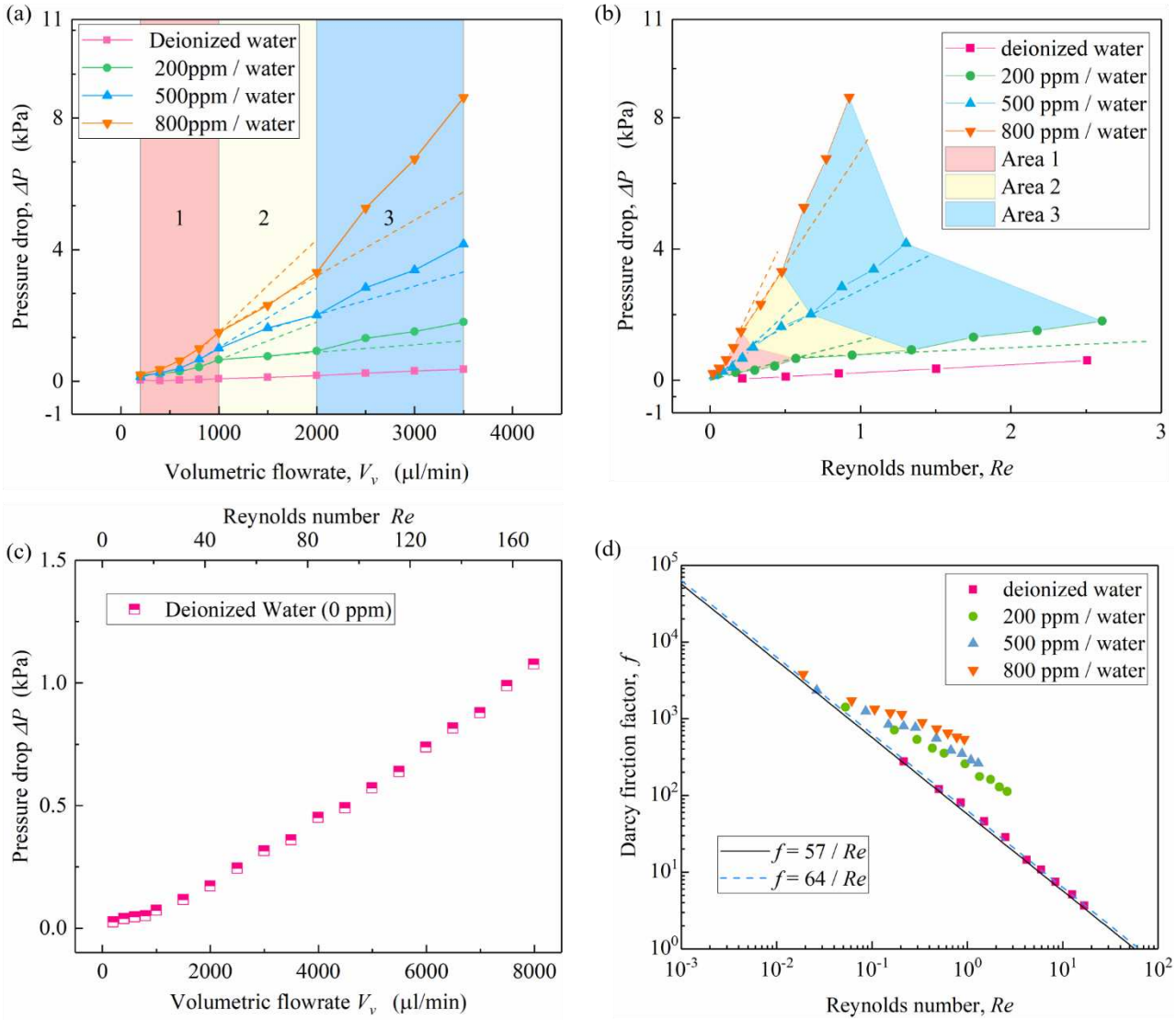

Fig. 8 Pressure drops variations. (a) The dependence of pressure drops ΔP of deionized water on volumetric flowrates V_V. (b) The dependence of pressure drops ΔP of deionized water on Reynolds number Re. (c) The dependence of pressure drops ΔP on volumetric flowrates V_V from 200 μl/min to 3500 μl/min of Deionized water. (d) The dependence of Darcy friction factor f on Reynolds number Re.

3.3 Axial profiles of the convective heat transfer coefficient

In the following, the heat transfer performance of shear-thinning fluids flow with a particular attention on the cases showing the effects of elastic instability and elastic influence is analyzed.

Fig. 9 shows the variations of temperatures. The dependence of inlet and outlet temperatures on polymer concentrations are illustrated in Fig. 9 (a) and also the averaged inlet and outlet temperatures of different polymer concentrations. One can see that the outlet temperatures decline slightly with the polymer concentration as which the inlet temperature has a small fluctuation which predicted that the heat flux keep constant for various polymer concentrations. Fig. 9 (b) shows wall temperature of the deionized water against Dimensionless axial distance. Fig. 9 (c) and Fig. 9 (d) show wall temperatures versus dimensionless axial distance at $Re = 0.6 \pm 0.05$ and $Re = 0.9 \pm 0.04$, respectively. Wall temperature increases along the channel and becomes lower with an increased Reynolds number. Fig.

10 shows the dependence of the local convective heat transfer coefficient h on the dimensionless axial distance X/a for a Newtonian fluid and shear-thinning fluids at $Re = 0.6 \pm 0.05$ and $Re = 0.9 \pm 0.04$, respectively.

In the flows of Newtonian fluid (deionized water), the convective heat transfer coefficient h is approximately constant with the increased dimensionless axial distance which means that the flow are fully developed for the Newtonian fluids. Here, since that the flow within the serpentine channel is laminar flow as schematically showed in Fig. 7, the length of the entrance region can be predicted by the equation $l/d \approx 0.05RePr$[43], approximately from 0.3 to 1.2 here, which means that for the tested points along the channel, the flow of Newtonian fluid are fully developed. However, for shear-thinning fluids, the results are different. The local heat transfer coefficient h of shear-thinning fluids increases non-linearly along the serpentine channel with dimensionless axial distance X/a from Position1 to Position4. A sharp growth of the local heat transfer coefficient for shear-thinning fluids has been observed in higher PAAm concentration in Fig. 10 (c) and (d). In addition, with the enhancement of Reynolds number, a moderate increase of local convective heat transfer coefficients is observed when Fig. 10 (a) and Fig. 10 (b) are compared.

In the flows of shear-thinning fluids, due to the addition of polymer into the working fluids, the viscosity of solutions are significantly improved as illustrated previously (refer to *section 2.4 Polyacrylamide polymer solutions*) which means that the length of entrance region of the serpentine channel is strongly enhanced and leads to a developing flow within the channel. In this condition, if the polymer flow is a laminar flow, the local surface heat transfer coefficient should decline along the channel within the entrance region. However, as illustrated in Fig. 10 (a) and Fig. 10 (b), the local heat transfer coefficient enhances with the dimensionless axial distance which shows that the local heat transfer performance is affected by the generation of elastic instability and elastic turbulence. In the flow of polymer solutions, the thermal and flow boundary layer are both affected by the induction of elastic turbulence and elastic instability which leading to an increased perturbation and intensified mixing. The interaction of turbulent perturbation and mixing effects causes the enhancement of local surface heat transfer coefficient with in the region of developing turbulent flow.

Furthermore, a non-linear enhancement were observed in Fig. 10 (a) and Fig. 10 (b). The strong non-linearity in the flow within the serpentine channel indicates that the induced elastic instability indeed affects local heat transfer performance and confirms that PAAm concentration is able to influence magnitudes of elastic instability. Within the serpentine channel, the pure Newtonian fluids (deionized water) is remaining in laminar regime without any sharp and non-linear variations of local heat transfer coefficients during the experimental test, which indicates that the inertial effect in this situation is negligible and the enhanced heat transfer performance is independently driven by the elastic instability, similar to previous studies[20,35]. However, the moderate enhancement of local heat transfer coefficients do exist when one is comparing Fig. 10 (a) and (b) which means that probably the increased Reynolds number leads to a slight enhancement of heat transfer. Since that the quantity of increased Reynolds number is negligible in comparison with the enhanced Weissenberg number, the main effect of additional heat transfer are contributed to elastic effect.

Growth of the heat transfer coefficient is affected significantly by the addition of polymer particles. Similar to previous studies by Abed et al. [20] and Li et al. [35-37], the global heat transfer coefficient in the serpentine channel is enhanced. Furthermore, the local heat transfer discrepancy due to evolution

of the elastic turbulence has also been revealed. One can see from Fig. 10 (a) and (b) that even at lower PAAM concentration such as 200 ppm in this experiment, a non-linear heat transfer performance was observed in shear-thinning fluids along a serpentine channel which is attributed to the increased intensity of elastic instability[22,44] induced by the polymer elasticity along a serpentine channel. In comparison with previous studies on global heat transfer coefficients within serpentine channels, the non-linear trends of local heat transfer coefficients along the channel were observed in this studies which cannot be revealed solely by the global heat transfer investigations. The onset of non-linear instability has been attributed to a balance between normal stresses and streamline curvature and systematic studies of curvature effects of elastic instability are conducted by J. Zilz et al.[45]. The flow of polymer tends to be more unstable and the stress ratio reaches a higher value as the flow develops along the channel. The perturbation by streamline curvatures[45,46] of a serpentine channel enlarges elastic stress ratio of polymer due to the enhanced stretch of a single high-molecular-weight flexible polymer molecule and coil of multiple polymer molecules related to polymer twisting, convolutions and interactions within shear-thinning fluids which are detailly and systematically investigated in the polymer dynamic study associated with coil-stretch transition conducted by Gerashchenko et al.[47].

With increased polymer concentration, a higher heat transfer coefficient and a better heat transfer performance were detected in comparison with the lower polymer concentration, indicating that the intensity of elastic instability is involved with polymer concentrations. Although the viscosity of shear-thinning fluids related to dissipation via linear stress relaxation[12] increases with the enhancement of polymer concentration, the relaxation time of shear-thinning fluids representing the nonlinear elastic stress increases as well. With a higher polymer concentration, the polymer solution tends to be more sensitive and the stress ratio reaches a higher degree of perturbations induced by polymer twisting, convolutions and interaction, which agrees well with the investigations conducted by Jun and Steinberg[12,18] that the intensity of elastic instability reinforced with the increased polymer concentration.

At a higher Reynolds number, a moderately closer trend is observed between polymer solutions with the concentration of 500 ppm and 800 ppm compared to a lower Reynolds number(as shown in Fig. 10), which demonstrates that the elastic instability are influenced by the coupling of concentration effects and Reynolds effects. The dilute polymer solution responses more sensitive to Reynolds number while the semi-dilute polymer solution is obtuse as the concentration of a polymer solution reaches to the threshold of dilute and semi-dilute (here the threshold is approximately 550 ppm according to Qin and Arratia [21]). As the Reynold number increases, the onset of reduced differences between curves are attributed to the nearly saturated elastic stress resulting from the limited polymer stretching and coiling intensity in semi-dilute polymer solutions.

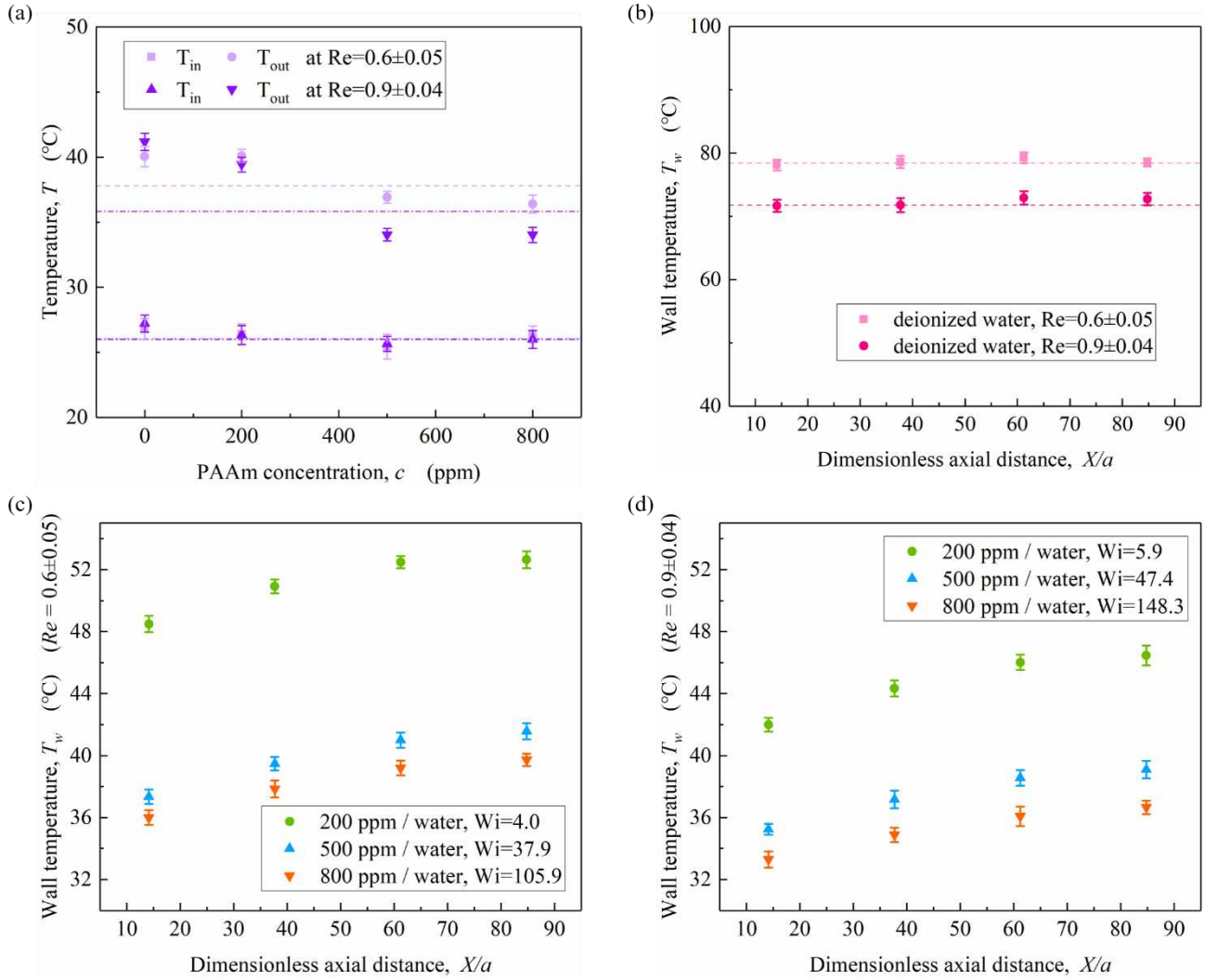

Fig. 9 Variations of temperatures. (a) Variations of inlet and outlet temperatures with PAAm concentration at $Re = 0.6 \pm 0.05$ and $Re = 0.9 \pm 0.04$, respectively. (b) Variations of wall temperatures of deionized water (0 ppm) with dimensionless axial distance X/a at $Re = 0.6 \pm 0.05$ and $Re = 0.9 \pm 0.04$, respectively. (c) Wall temperatures versus dimensionless axial distance X/a at $Re = 0.6 \pm 0.05$. (d) Wall temperatures versus dimensionless axial distance X/a at $Re = 0.9 \pm 0.04$.

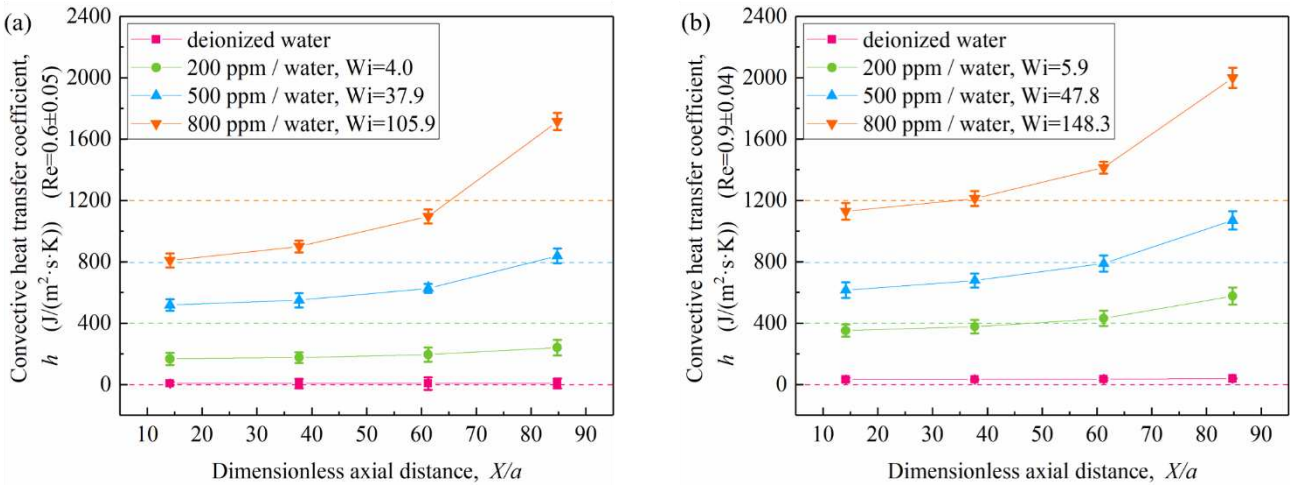

Fig. 10 Local convective heat transfer coefficient h of Newtonian fluids (deionized water) and shear-thinning fluids (200 ppm / Water, 500 ppm / Water and 800 ppm /Water) versus dimensionless axial distance X/a at $Re = 0.6 \pm 0.05$ and $Re = 0.9 \pm 0.04$, respectively.

3.4 Dependence of the Nusselt number on Weissenberg number, Reynolds number, Graetz number and shear rate

Dependence of the Nusselt number on shear rate and different dimensionless numbers, including Weissenberg number *Wi*, Reynolds number *Re* and Graetz number *Gz*, are shown in Fig. 11 to Fig. 16 and analyzed.

First, Fig. 11 shows the variations of Nusselt number *Nu* with Weissenberg number *Wi* at different positions for different polymer concentrations which are 200 ppm, 500 ppm, and 800 ppm, respectively. A significant enhancement of Nusselt number versus Weissenberg number are observed in Fig. 11 in different polymer concentrations. From Position1 to Position4, the difference of Nusselt number of between two adjacent positions become more significant and it is enhanced with Weissenberg number at the same time. Fig. 12 shows relations of Nusselt number *Nu* to Weissenberg number *Wi* of shear-thinning fluids with various concentrations at different positions from Position1 to Position4, respectively. It is clearly that the Nusselt number increases rapidly with Weissenberg number but more gently with a higher polymer concentration. In comparison with previous studies[19,20,35–37] of global heat transfer performance estimated by the dependence of mean Nusselt number on Weissenberg number, a detailed trends at fixed positions are conducted in this investigation. Such an enhancement is extremely possible caused by the addition of polymer and the existence of elasticity of the polymer molecule. At lower Weissenberg number, the polymer elasticity are not strong enough to induce elastic turbulence, but a weak bifurcation flow[48] are possible generated which results in a weak perturbation of the flow and leading to the weak enhancement of Nusselt number. With the enhancement of Weissenberg number, a creeping flow is developed and elastic instability is generated, resulting in a more significant enhancement of Nusselt number. After that, as the Weissenberg number reaches a higher value, with the development of perturbation, elastic turbulence is induced by the interaction between curvature and polymer elasticity which leading to a much higher Nusselt number and a higher rate of enhancement. Since that the polymer solution with a higher polymer concentration has a longer relaxation time, which means that the high concentration polymer solution has a more significant ability to be stretched but need more perturbations to be stretched. At a constant Weissenberg number, the degrees of polymer stretching are of the same value as mentioned by Varshney and Steinberg[49] , which means that the percentage of stretching of polymer molecules in polymer solution with low concentration are more significant than that in polymer solution with high concentration.

Second, The local Nusselt number versus Reynolds number at different positions with the polymer concentration of 200 ppm, 500 ppm, and 800 ppm, respectively, is shown in Fig. 13. It can be observed that the Nusselt number increases with the enhancement of Reynolds number. The difference between the adjacent positions become more significant from Position1 to Position4. The variations of local Nusselt number with Reynolds number with different concentration at positions from Position1 to Position4 are sown in Fig. 14. It is clear that Nusselt number increases more rapidly with the enhanced polymer concentration. Since that the inertial effects are not dominated effects in such flow, a different trend of the Nusselt number versus Reynolds number were observed in this experiments. The

Complicated competition between inertial stress and elastic stress leads to the reduction of drag and possibly results in the enhancement of elastic instability and elastic turbulence. When the inertial stress is at the same value, increased polymer concentration is the sign of enhanced elasticity associated with the elastic instability and elastic turbulence. Both of the intricate E-I competition[49] and enhanced elasticity are responsible for the enhancement of heat transfer performance.

In addition, The local Nusselt numbers versus shear rates of positions from Position1 to Position4 with the polymer concentration of 200 ppm, 500 ppm, 800 ppm, respectively, are illustrated in Fig. 15 (a) (b) and (c), respectively, which shows that the Nusselt number increases rapidly with an enhanced shear rate. From Position1 to Position4, the enhancement of Nusselt number become more rapid. The gap between Nusselt numbers of the adjacent positions is extended as the shear rate is enhanced. The dependence of Nusselt number on shear rate of different polymer concentrations at Position4 is also shown in Fig. 15 (d). It is clear that the addition of polymer do enhanced the heat transfer performance which increase with the polymer concentration. And at last, the local Nusselt numbers *Nu* for the Newtonian solution (deionized water) and shear-thinning fluids against Graetz number *Gz* at Position4 (X/a = 84.8) are shown in Fig. 16 (b) while the dependence of Nusselt numbers on Graetz number at different positions are schematically shown in Fig. 16 (a). It is obvious that at low Graetz number, the curvature of the serpentine channel has limited influence on the Newtonian fluid flow. Oppositely, a significant enhancement of Nusselt number do exist for the shear-thinning fluids. Similar trends are observed between Fig. 15 (b) and Fig. 16 (a) and between Fig. 15 (d) and Fig. 16 (b) since that the Graetz number is proportional to the shear rate which represents the flow development and point to the purely elastic instability in creeping shear thinning fluids. Since that the centrifugal effects and related Dean number are not large enough to cause the Dean effects, the reason for the enhancement of heat transfer performance are mainly attributed to the shear-thinning effects within the serpentine flow.

It is expected that the increase are caused by elastic instability and elastic turbulence. In comparison with the dependence of mean Nusselt number on Weissenberg number and Graetz number illustrated by Li et al. [35], a similar trend were observed in Fig. 12 and Fig. 16 with the range of Weissenberg number from approximately 0.7 to 14.0 at different positions along the channel. A higher Nusselt number were showed in their results for the possible reasons that a serpentine channel with a smaller scale and more segments were utilized in their experiments, different polyacrylamide were used for the addition of the working fluids and the flow is developing in our investigation. The small scale probably has benefits on the overall heat transfer while PAAm and NPAM (nonionic polyacrylamide used by Li et al. [35]) has different heat transfer performance and it seems that NPAM has a better heat transfer performance which indicates that the existence of anions has a negative effects on the heat transfer performance.

The strong increase of Nusselt number with a higher Weissenberg number and lower PAAm concentration indicates that the induced elastic instability intensify the heat transfer performance along a serpentine channel, which agrees well with investigations conducted by Li et al.[35] that the Nusselt number sharply increases with Weissenberg number exceeds the critical value of 2.1. As the experimental Weissenberg number in this study is much larger than the referenced critical value, it is reasonable to consider that the elastic instability is indeed aroused in the flow. Correspondence between *Nu* and *Wi* is also systematical investigated in serpentine channels by Abed et al.[20] and his co-workers

under the boundary condition of constant wall temperature with *Wi* from extremely low to approximately 250 that the mean Nusselt number increases with Weissenberg number and decreases with polymer concentration. However, the onset value of Wi in their study is estimated as $Wi = 25$ which is much higher than that is deduced by Li et al.[35]. Such a difference is probably caused by different scales of their serpentine channels and working fluids used in experimental systems. Although the critical Wi is different in their studies, both of their studies conclude that the dramatical increase of Nusselt number versus Weissenberg number indicates the induction of elastic instability and elastic turbulence in the serpentine flow of shear-thinning fluids do strongly affect the heat transfer performance. It is expected that the heat transfer performance of a fixed position is enhanced and interacted by elastic instability[18].

Enhancement of the Nusselt number is influenced significantly by the addition of polymer. At lower polymer concentration, the Nusselt number increases more steeply with the Weissenberg number which can be attributed to the shorter relaxation time. The relaxation time influences the onset and intensity of elastic instability in serpentine flows by affecting the amplitudes and frequencies of molecule stretching and coiling. It is expected that a coupling of relaxation effects and elastic instability determines the heat transfer performance characterized by the Nusselt number related to the Weissenberg number which has different critical values and strongly affects the onset of elastic turbulence as is systematically investigated by Jun and Steinberg[50] in their studies.

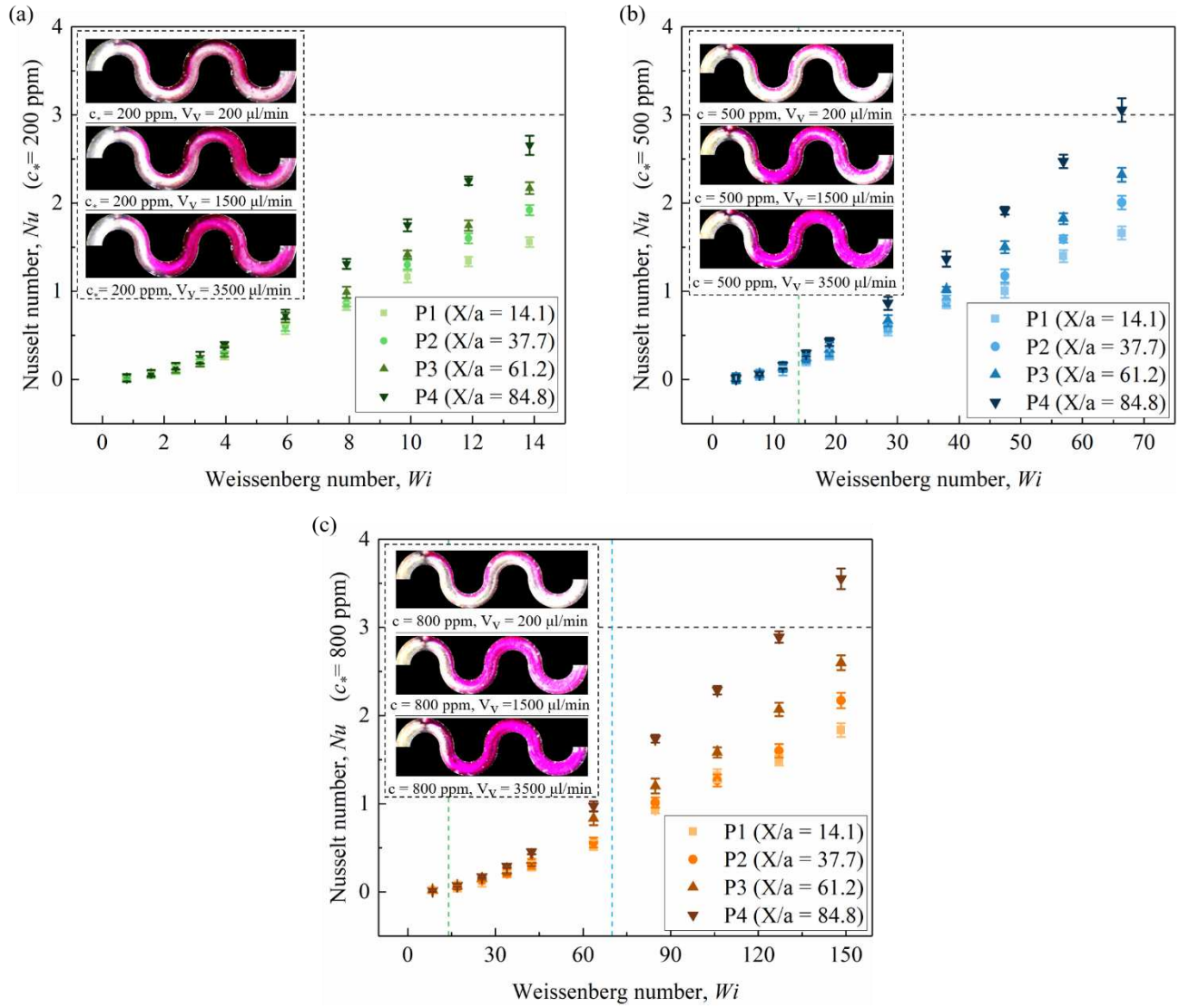

Fig. 11 The dependence of Nusselt number, *Nu*, on Weissenberg number, *Wi*, at different PAAm concentrations. (a) Nusselt number against Weissenberg number of PAAm aqueous solution with the concentration of 200 ppm. (b) Nusselt number against Weissenberg number of PAAm aqueous solution with the concentration of 500 ppm. (c) Nusselt number against Weissenberg number of PAAm aqueous solution with the concentration of 800 ppm.

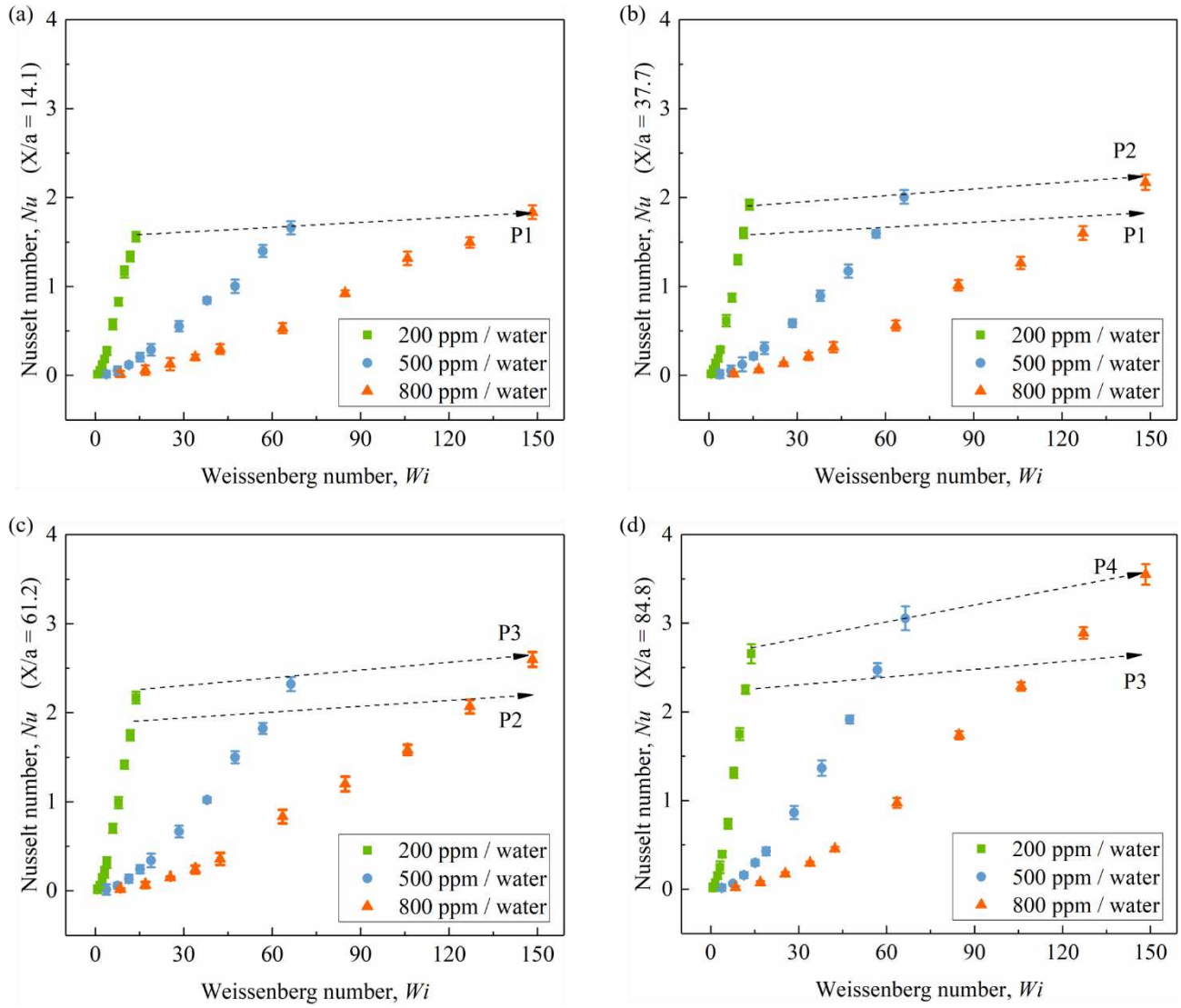

Fig. 12 Nusselt number, *Nu*, versus Weissenberg number, *Wi*, at different positions. (a) Nusselt number versus Weissenberg number at Position1 ($X/a = 14.1$) (b) Nusselt number versus Weissenberg number at Position2 ($X/a = 37.7$) (c) Nusselt number versus Weissenberg number at Position3 ($X/a = 61.2$) (d) Nusselt number versus Weissenberg number at Position4 ($X/a = 84.8$).

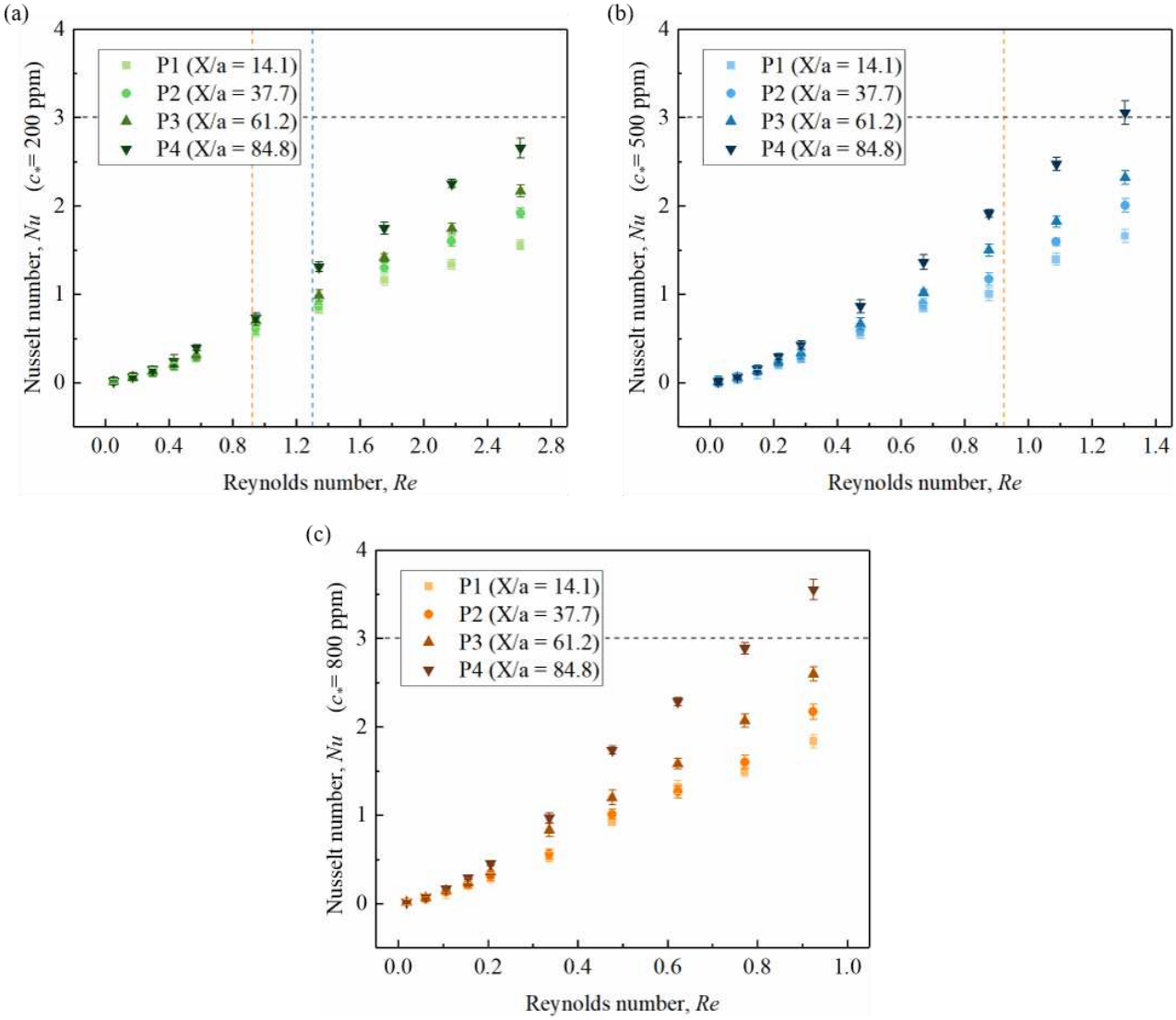

Fig. 13 The dependence of Nusselt number, *Nu*, on Reynolds number, *Re*, at different PAAm concentrations.
(a) Nusselt number against Reynolds number of PAAm aqueous solution with the concentration of 200 ppm.
(b) Nusselt number against Reynolds number of PAAm aqueous solution with the concentration of 500 ppm.
(c) Nusselt number against Reynolds number of PAAm aqueous solution with the concentration of 800 ppm.

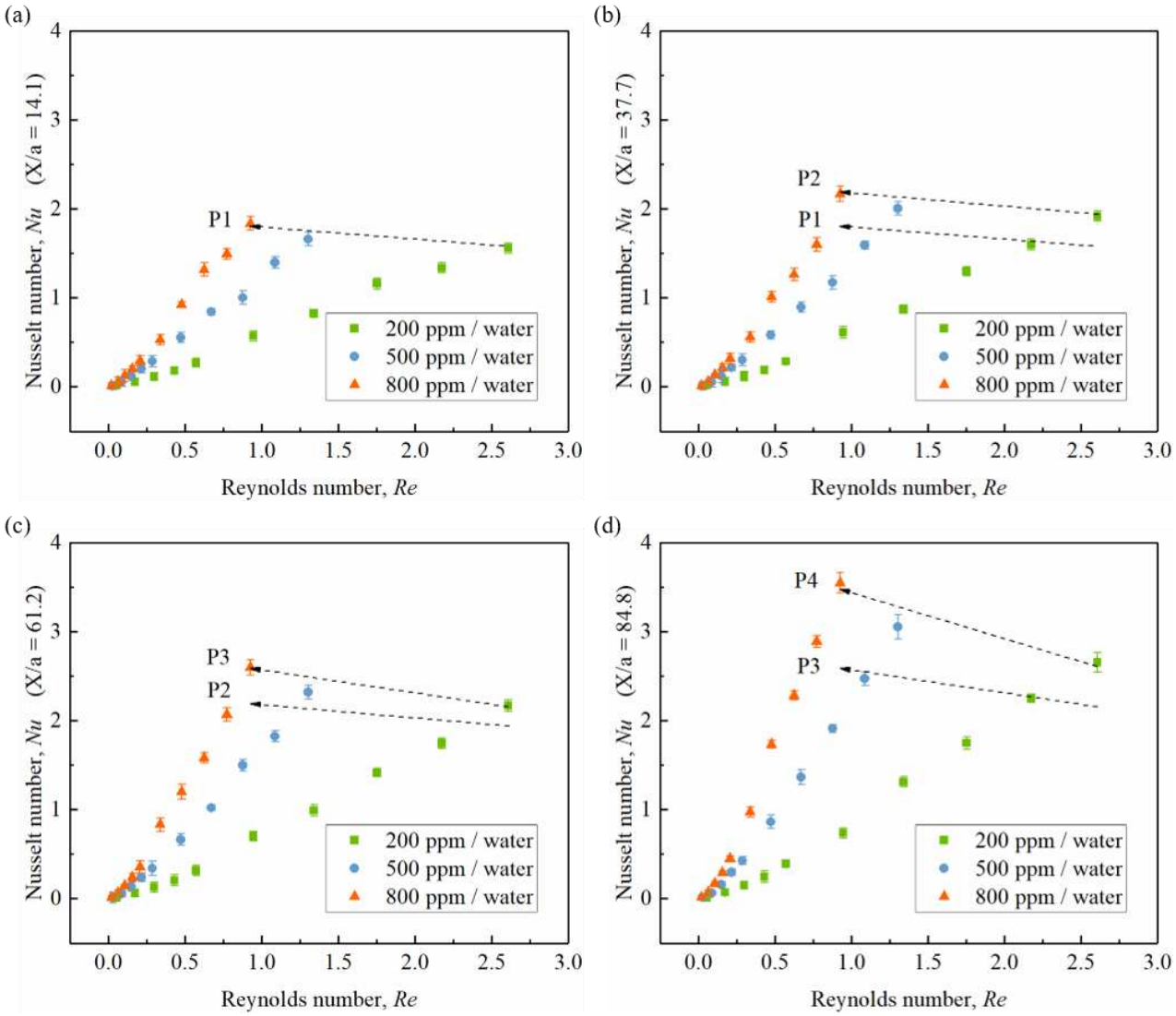

Fig. 14 Local Nusselt number, *Nu*, versus Reynolds number, *Re*, for PAAm aqueous solutions. (a) Nusselt number versus Reynolds number at Position1 ($X/a = 14.1$) (b) Nusselt number versus Reynolds number at Position2 ($X/a = 37.7$) (c) Nusselt number versus Reynolds number at Position3 ($X/a = 61.2$) (d) Nusselt number versus Reynolds number at Position4 ($X/a = 84.8$).

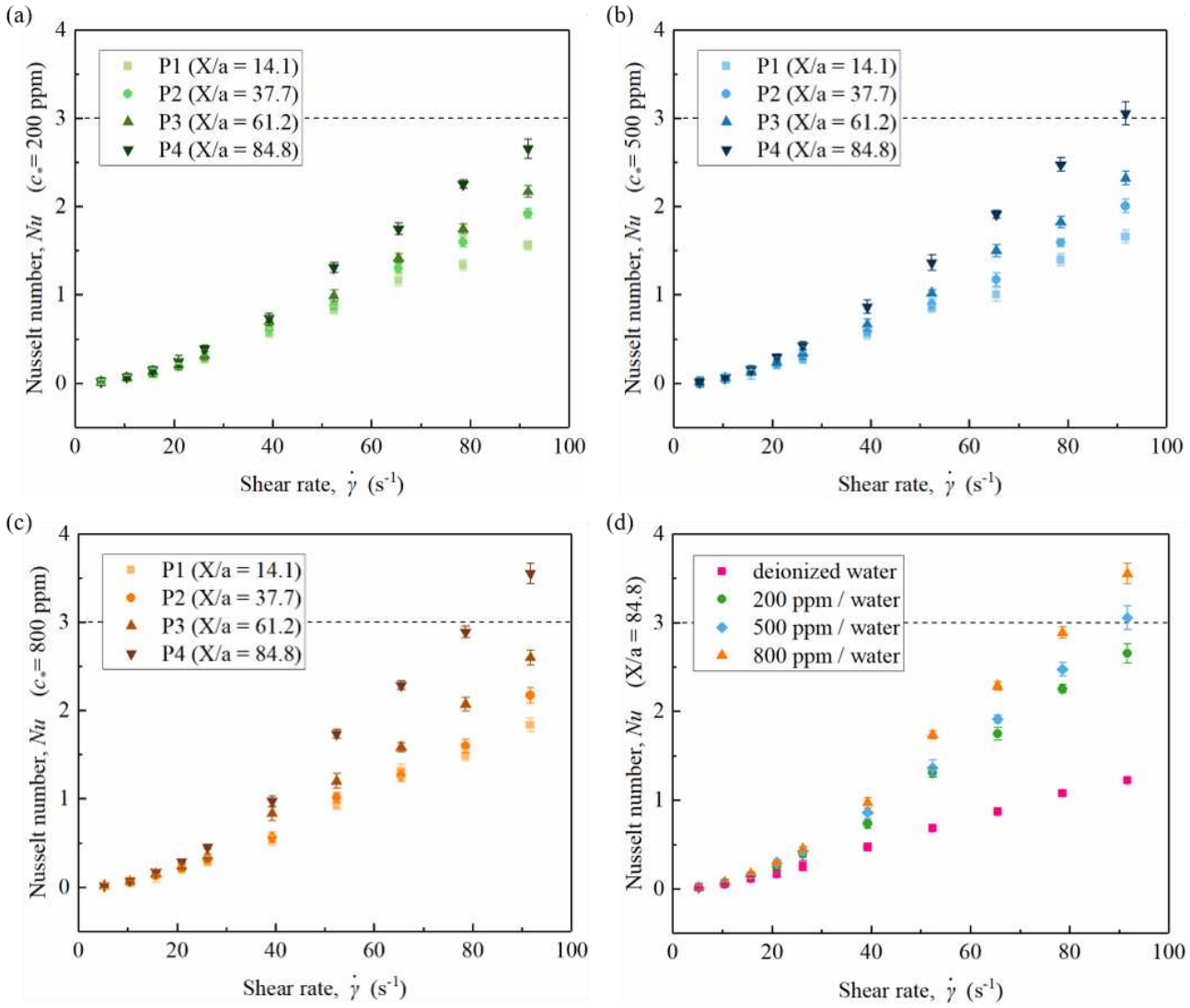

Fig. 15 Local Nusselt number, Nu, verus shear rate, $\dot{\gamma}$, for deionized water and PAAm aqueous solutions. (a) The dependence of local Nusselt number on shear rate of the polymer solution with the concentration of 200 ppm, 500 ppm, and 800 ppm at Positions from Position1 (X/a = 14.1) to Position4 (X/a = 84.8), respectively. (b) The dependence of local Nusselt number on shear rate of the deionized water and the polymer solution with concentrations of 200 ppm, 500 ppm, and 800 ppm, respectively, at Position4 (X/a = 84.8).

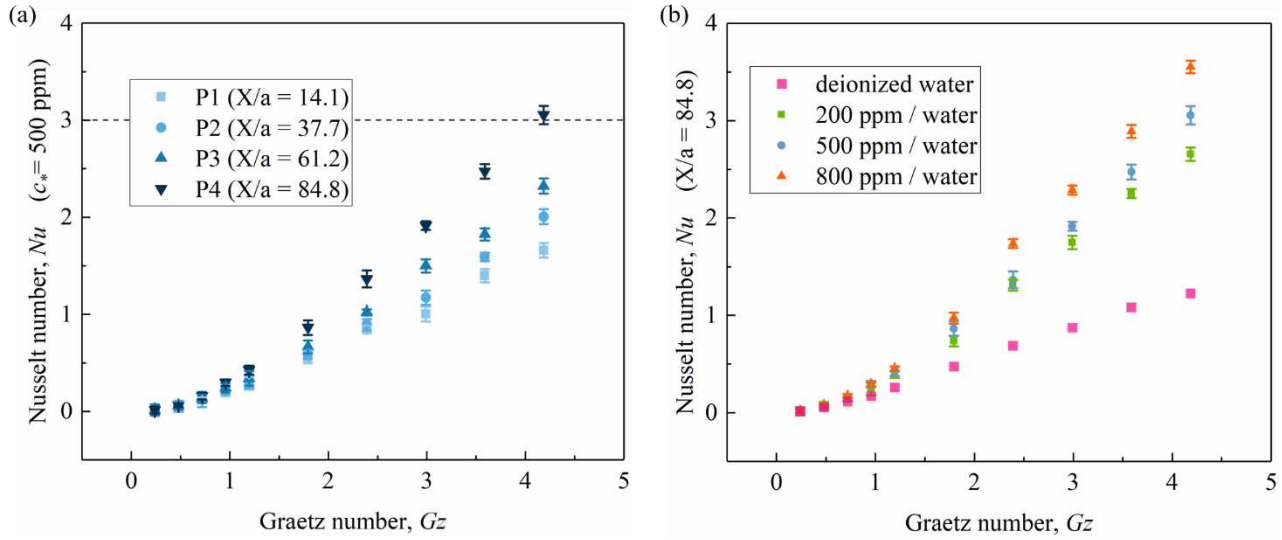

Fig. 16 Local Nusselt number, *Nu*, verus Graetz number, *Gz*, for deionized water and PAAm aqueous solutions. (a) The dependence of local Nusselt number on Graetz number of the polymer solution with the concentration of 500 ppm at Positions from Position1 (X/a = 14.1) to Position4 (X/a = 84.8). (b) The dependence of local Nusselt number on Graetz number of the polymer solution with concentrations of 200 ppm, 500 ppm, and 800 ppm, respectively, at Position4 (X/a = 84.8).

4 Conclusions

The flow visualization and local convective heat transfer performance by elastic turbulence have been investigated experimentally in a serpentine channel with shear-thinning fluids. A strong evidence, which is the dramatically enhanced mixing effect as shown in the flow visualization results, is given for the generation of elastic instability and elastic turbulence in the serpentine channel. A three-stage pressure drop profile is identified due to the high viscosity at low flowrates, shear-thinning properties at medium flowrates and elastic turbulence at high flowrates. With increasing dimensionless axial distance, the local heat transfer coefficient increases non-linearly, resulting in a higher heat transfer performance. Owing to gradually increased intensity of elastic instability attributed to the interactions between normal stresses and streamline curvature along a serpentine channel, a non-linear heat transfer performance is observed. Particularly, a higher intensity of elastic instability is developed at a higher polymer concentration where the polymer solution tends to be more sensitive and the stress ratio reaches a higher degree of perturbations induced by polymer twisting, convolutions and interaction. A steeper increase of local Nusselt number with Weissenberg number at lower polymer concentrations is ascribed to the coupling of elastic instability and shear-thinning effects related to the rheological properties of polymer solutions.

Acknowledgments

The work is supported by NSFC under Grants 51876006.

References

[1] J.Z. Hilt, N.A. Peppas, Microfabricated drug delivery devices, Int. J. Pharm. 306 (2005) 15–23.

[2] S.Z. Razzacki, P.K. Thwar, M. Yang, V.M. Ugaz, M.A. Burns, Integrated microsystems for controlled drug delivery, Adv. Drug Deliv. Rev. 56 (2004) 185–198.

[3] R.S. Shawgo, A.C.R. Grayson, Y. Li, M.J. Cima, BioMEMS for drug delivery, Curr. Opin. Solid State Mater. Sci. 6 (2002) 329–334.

[4] S.S. Mehendale, A.M. Jacobi, R.K. Shah, Fluid flow and heat transfer at micro-and meso-scales with application to heat exchanger design, Appl. Mech. Rev. 53 (2000) 175–193.

[5] M. Meis, F. Varas, A. Velázquez, J.M. Vega, Heat transfer enhancement in micro-channels caused by vortex promoters, Int. J. Heat Mass Transf. 53 (2010) 29–40.

[6] R.M. Bryce, M.R. Freeman, Abatement of mixing in shear-free elongationally unstable viscoelastic microflows, Lab. Chip. 10 (2010) 1436–1441.

[7] S. Shen, J.L. Xu, J.J. Zhou, Y. Chen, Flow and heat transfer in microchannels with rough wall surface, Energy Convers. Manag. 47 (2006) 1311–1325.

[8] O.I. Rovenskaya, G. Croce, Heat transfer in rough microchannels under rarefied flow conditions, Eur. J. Mech.-BFluids. 72 (2018) 706–715.

[9] J.L. Xu, Y.H. Gan, D.C. Zhang, X.H. Li, Microscale heat transfer enhancement using thermal boundary layer redeveloping concept, Int. J. Heat Mass Transf. 48 (2005) 1662–1674.

[10] A. Groisman, V. Steinberg, Elastic turbulence in a polymer solution flow, Nature. 405 (2000) 53.

[11] A. Groisman, V. Steinberg, Efficient mixing at low Reynolds numbers using polymer additives, Nature. 410 (2001) 905.

[12] Y. Jun, V. Steinberg, Polymer concentration and properties of elastic turbulence in a von Karman swirling flow, Phys. Rev. Fluids. 2 (2017) 103301.

[13] T. Burghelea, E. Segre, V. Steinberg, Role of elastic stress in statistical and scaling properties of elastic turbulence, Phys. Rev. Lett. 96 (2006) 214502.

[14] A. Groisman, V. Steinberg, Elastic turbulence in curvilinear flows of polymer solutions, New J. Phys. 6 (2004) 29.

[15] T. Burghelea, E. Segre, I. Bar-Joseph, A. Groisman, V. Steinberg, Chaotic flow and efficient mixing in a microchannel with a polymer solution, Phys. Rev. E. 69 (2004) 066305.

[16] A. Souliès, J. Aubril, C. Castelain, T. Burghelea, Characterisation of elastic turbulence in a serpentine micro-channel, Phys. Fluids. 29 (2017) 083102.

[17] F.-C. Li, H. Kinoshita, X.-B. Li, M. Oishi, T. Fujii, M. Oshima, Creation of very-low-Reynolds-number chaotic fluid motions in microchannels using viscoelastic surfactant solution, Exp. Therm. Fluid Sci. 34 (2010) 20–27.

[18] Y. Jun, V. Steinberg, Elastic turbulence in a curvilinear channel flow, Phys. Rev. E. 84 (2011) 056325.

[19] R.D. Whalley, W.M. Abed, D.J.C. Dennis, R.J. Poole, Enhancing heat transfer at the micro-scale using elastic turbulence, Theor. Appl. Mech. Lett. 5 (2015) 103–106.

[20] W.M. Abed, R.D. Whalley, D.J. Dennis, R.J. Poole, Experimental investigation of the impact of elastic turbulence on heat transfer in a serpentine channel, J. Non-Newton. Fluid Mech. 231 (2016) 68–78.

[21] B. Qin, P.E. Arratia, Characterizing elastic turbulence in channel flows at low Reynolds number, Phys. Rev. Fluids. 2 (2017).

[22] L. Pan, A. Morozov, C. Wagner, P.E. Arratia, Nonlinear elastic instability in channel flows at low Reynolds numbers, Phys. Rev. Lett. 110 (2013) 174502.

[23] Y. Liu, V. Steinberg, Molecular sensor of elastic stress in a random flow, EPL Europhys. Lett. 90 (2010) 44002.

[24] A. Groisman, V. Steinberg, Stretching of polymers in a random three-dimensional flow, Phys. Rev. Lett. 86 (2001) 934.

[25] Y. Liu, V. Steinberg, Stretching of polymer in a random flow: Effect of a shear rate, EPL Europhys. Lett. 90 (2010) 44005.

[26] S. Berti, G. Boffetta, Elastic waves and transition to elastic turbulence in a two-dimensional viscoelastic Kolmogorov flow, Phys. Rev. E. 82 (2010) 036314.

[27] M.M. Afonso, D. Vincenzi, Nonlinear elastic polymers in random flow, J. Fluid Mech. 540 (2005) 99–108.

[28] T. Burghelea, E. Segre, V. Steinberg, Mixing by polymers: Experimental test of decay regime of mixing, Phys. Rev. Lett. 92 (2004) 164501.

[29] H.Y. Gan, Y.C. Lam, N.T. Nguyen, K.C. Tam, C. Yang, Efficient mixing of viscoelastic fluids in a microchannel at low Reynolds number, Microfluid. Nanofluidics. 3 (2007) 101–108.

[30] H.Y. Gan, Y.C. Lam, N.-T. Nguyen, Polymer-based device for efficient mixing of viscoelastic fluids, Appl. Phys. Lett. 88 (2006) 224103.

[31] K. Tatsumi, Y. Takeda, K. Suga, K. Nakabe, Turbulence characteristics and mixing performances of viscoelastic fluid flow in a serpentine microchannel, in: J. Phys. Conf. Ser., IOP Publishing, 2011: p. 092020.

[32] L. Casanellas, M.A. Alves, R.J. Poole, S. Lerouge, A. Lindner, The stabilizing effect of shear thinning on the onset of purely elastic instabilities in serpentine microflows, Soft Matter. 12 (2016) 6167–6175.

[33] R.J. Poole, B. Budhiraja, A.R. Cain, P.A. Scott, Emulsification using elastic turbulence, J. Non-Newton. Fluid Mech. 177 (2012) 15–18.

[34] B. Traore, C. Castelain, T. Burghelea, Efficient heat transfer in a regime of elastic turbulence, J. Non-Newton. Fluid Mech. 223 (2015) 62–76.

[35] D.-Y. Li, X.-B. Li, H.-N. Zhang, F.-C. Li, S. Qian, S.W. Joo, Efficient heat transfer enhancement by elastic turbulence with polymer solution in a curved microchannel, Microfluid. Nanofluidics. 21 (2017) 10.

[36] D.-Y. Li, X.-B. Li, H.-N. Zhang, F.-C. Li, S.-Z. Qian, S.W. Joo, Measuring heat transfer performance of viscoelastic fluid flow in curved microchannel using Ti–Pt film temperature sensor, Exp. Therm. Fluid Sci. 77 (2016) 226–233.

[37] D. Li, X. Li, F. Li, Heat Transfer Enhancement of Elastic Turbulence in Curved Microchannel, in: ASMEJSMEKSME 2015 Jt. Fluids Eng. Conf., American Society of Mechanical Engineers, 2015: p. V002T10A002–V002T10A002.

[38] D. Copeland, C. Ren, M. Su, P. Ligrani, Elastic turbulence influences and convective heat transfer within a miniature viscous disk pump, Int. J. Heat Mass Transf. 108 (2017) 1764–1774.

[39] M.P. Escudier, I.W. Gouldson, A.S. Pereira, F.T. Pinho, R.J. Poole, On the reproducibility of the rheology of shear-thinning liquids, J. Non-Newton. Fluid Mech. 97 (2001) 99–124.

[40] P.M. Ligrani, S. Choi, A.R. Schallert, P. Skogerboe, Effects of Dean vortex pairs on surface heat transfer in curved channel flow, Int. J. Heat Mass Transf. 39 (1996) 27–37.

[41] P.M. Ligrani, C.R. Hedlund, Experimental Surface Heat Transfer and Flow Structure in a Curved Channel With Laminar, Transitional, and Turbulent Flows, J. Turbomach. 126 (2004) 414–423. https://doi.org/10.1115/1.1738119.

[42] W.M. Abed, R.D. Whalley, D.J.C. Dennis, R.J. Poole, Numerical and experimental investigation of heat transfer and fluid flow characteristics in a micro-scale serpentine channel, Int. J. Heat Mass Transf. 88 (2015) 790–802. https://doi.org/10.1016/j.ijheatmasstransfer.2015.04.062.

[43] D. Wen, Y. Ding, Experimental investigation into convective heat transfer of nanofluids at the entrance region under laminar flow conditions, Int. J. Heat Mass Transf. 47 (2004) 5181–5188.

[44] P.C. Sousa, F.T. Pinho, M.A. Alves, Purely-elastic flow instabilities and elastic turbulence in microfluidic cross-slot devices, Soft Matter. 14 (2018) 1344–1354.

[45] J. Zilz, R.J. Poole, M.A. Alves, D. Bartolo, B. Levaché, A. Lindner, Geometric scaling of a purely elastic flow instability in serpentine channels, J. Fluid Mech. 712 (2012) 203–218.

[46] S. Khorasani, S. Jafarmadar, S. Pourhedayat, M.A.A. Abdollahi, A. Heydarpour, Experimental investigations on the effect of geometrical properties of helical wire turbulators on thermal performance of a helically coiled tube, Appl. Therm. Eng. 147 (2019) 983–990.

[47] S. Gerashchenko, C. Chevallard, V. Steinberg, Single-polymer dynamics: Coil-stretch transition in a random flow, EPL Europhys. Lett. 71 (2005) 221.

[48] S. Belan, A. Chernykh, V. Lebedev, Boundary layer of elastic turbulence, J. Fluid Mech. 855 (2018) 910–921.

[49] A. Varshney, V. Steinberg, Drag enhancement and drag reduction in viscoelastic flow, Phys. Rev. Fluids. 3 (2018) 103302.

[50] Y. Jun, V. Steinberg, Power and pressure fluctuations in elastic turbulence over a wide range of polymer concentrations, Phys. Rev. Lett. 102 (2009) 124503.